Impedance Probe Payload Development for Space-Based Joint Service Collaboration

THESIS

Brian T. Kay, 1LT, USAF

AFIT-ENP-MS-21-M-121

DEPARTMENT OF THE AIR FORCE
AIR UNIVERSITY

AIR FORCE INSTITUTE OF TECHNOLOGY

Wright-Patterson Air Force Base, Ohio

AFIT-ENP-MS-21-M-121

Impedance Probe Payload Development for Space-Based Joint Service Collaboration

THESIS

Presented to the Faculty

Department of Engineering Physics

Graduate School of Engineering and Management

Air Force Institute of Technology

Air University

Air Education and Training Command

In Partial Fulfillment of the Requirements for the

Degree of Master of Science in Applied Physics

Brian T. Kay, B.S.

1LT, USAF

March 2021

AFIT-ENP-MS-21-M-121

Impedance Probe Payload Development for Space-Based Joint Service Collaboration

Brian T. Kay, B.S.

1LT, USAF

Committee Membership:

CDR R. James, Ph.D.
Chair

Maj D. Emmons, Ph.D.
Member

Dr. E. Tejero, Ph.D.
Member

Dr. M. McHarg, Ph.D.
Member

AFIT-ENP-MS-21-M-121

Abstract

Collaborations utilizing small spacecraft in near earth orbit between the U. S. Coast Guard Academy (CGA), Naval Research Lab (NRL), the U. S. Naval Academy (USNA), and the Air Force Institute of Technology (AFIT) have initiated scientific and engineering space-based experiments. Sourced opportunities like the VaSpace ThinSat missions have provided a platform for payload, sensor, and experiment development that would have otherwise been resource prohibitive. We have constructed an impedance probe payload derived from the existing 'Space PlasmA Diagnostic suitE' (SPADE) mission operating from NASA's International Space Station. Currently both space and laboratory plasmas are investigated with AC impedance measurements using a radio frequency antenna. Plasma electron density data collected from the ThinSat will however use an innovative surface-mounted dipole antenna to gather the required sheath-plasma and plasma resonance information. Results from this experiment will provide the framework for a CGA CubeSat with an impedance probe payload set to launch in late 2021. Impedance probe optimization, data collection obstacles, solutions, and procedures will be reported.

Acknowledgments

I would like to express my deepest appreciation to my family for their love and support during my studies. I could not be prouder of my wife who has managed to homeschool our three children during a pandemic while keeping me focused at the same time. I would also like to thank my children for their numerous and much needed entertainment during this difficult time.

I would also like to sincerely thank Commander Royce James for all his support and guidance throughout my master's program. Thank you for introducing me to an area of research that I find fascinating and hope to continue. I also want to thank my entire research committee for their numerous contributions and willingness to help me advance my academic career.

Lastly, I want to thank all the physics master's students who helped me along the way. It was a daunting task to attempt a master's program after an almost ten year break from academics. I could not have made it through without the help of the other two members of the Space Physics program, Seth Garland and Rodney Carmona.

Table of Contents

Page

List of Figures

List of Tables

Impedance Probe Payload Development for Space-Based Joint Service Collaboration

Introduction

Humanities excursion into space has become more than a symbol of prosperity and prowess. Recent advances in private and military space frameworks and infrastructures has galvanized our efforts to explore, maintain, and thrive in space. Real-time measurements of space plasmas are now possible on scale never seen before. Our goal is to demonstrate that for a fraction of the cost of a traditional satellite, we can build and deploy space plasma measuring payloads.

1.1 U.S. Space System Capabilities Enhanced with Accurate Plasma Parameters

The United States (U.S.) and U.S. Air Force depend on understanding the space environment. The space environment is an enormously complex system that has a direct impact on U.S. defense capabilities. Dependence on satellites continues to grow, as does the number of space systems in operation. All space systems operate in the harsh space environment and are subject to unpredictable space weather events. It is becoming vital to better understand the environment our satellites operate in and this can be achieved by improving U.S. capabilities to measure the plasma environment. The vast majority of all Low Earth Orbit (LEO) Satellites operate in the ionosphere which is a low-density, weakly ionized plasma region that ranges from 60 km to 1000 km (Schunk and Nagy, 2009).

Plasma is the most prevalent state of matter in the universe and is usually found in a vacuum environment or in stars. A plasma is a “quasineutral gas of charged and neutral

particles which exhibits collective behavior" (Chen, 2015). The motion of the charged particles creates localized electric fields and currents which in turn generates magnetic fields (Chen, 2015). Most space weather in our solar system is driven by the Sun. The Sun is capable violently ejecting plasma in an event known as a Coronal Mass Ejection (CME) (Russell, 2016). A CME is capable of reaching the Earth's magnetosphere and ionosphere potentially causing significant damage to satellites and other sensitive electronic equipment. The plasma environment with its varying electric currents can cause charge buildup on satellites. This is known as spacecraft charging and it can cause damage or destroy the satellite if not mitigated (NESC, 2016). Accurate, real-time measurements of plasma density and temperature are needed to help prevent spacecraft failure due to charging.

Satellite communications and long-range communications require an electromagnetic signal to either reflect off or propagate through the ionosphere. The plasma density in the ionosphere is a key parameter for determining the capability of these communications (Pisacane, 2008). Certain ionospheric conditions could lead to signal degradation or completely absorb it. Additionally, the density of space plasmas is primarily a factor of solar activity. Solar winds from the Sun are the primary driver for all space weather in our solar system (Russell, 2016). Having additional real-time, space-based in-situ plasma density measuring satellites will improve U.S. satellite communication capabilities and global space weather monitoring and characterization.

1.2 Ionospheric Environment

Ionospheric parameters are measured with several ground and space-based systems to provide near real-time data (Pisacane, 2008). There are a variety of models that provide

a global picture of the ionosphere available to the public. Space-based constellations that measure ionospheric characteristics are much more rare than ground-based systems. The recently launched Constellation Observing Satellite for Meteorology, Ionosphere, and Climate (COSMIC-2) and GPS constellation provide near real-time global ionospheric measurements. However, many more additional space-based in-situ sensors are needed to accurately measure and model the ionosphere.

The ionosphere contains a significant number of free electrons and ions that are primarily produced via extreme ultraviolet or EUV radiation from the Sun. Once ionized the electrons and ions are exposed to several different processes including chemical reactions, diffusion, plasma instabilities, and transport due to electric and magnetic fields. This forms a weakly ionized plasma (Schunk and Nagy, 2009). In the ionosphere the plasma density varies drastically with altitude and peaks around 350 km then begins to decrease. Dominant ion concentration, day/night cycle, latitude, longitude, and solar activity are several key factors that determine what the plasma density will be (Pisacane, 2008).

1.3 Current and future impedance probe effort

With the cost of launching to space constantly decreasing, access to space is becoming easier for a wide variety of organizations. Research organizations that were traditionally limited to ground-based labs can now conduct space-based research. The United States Coast Guard Academy (USCGA), Naval Research Labs (NRL), the U. S. Naval Academy (USNA), and the Air Force Institute of Technology (AFIT) have initiated a scientific and engineering space-based collaboration effort. We have partnered with Virginia Space's (VaSpace) ThinSat missions that will provided a platform for payload,

sensor, and experiment development that would have otherwise been resource prohibitive (James et al., 2020). We have constructed an impedance probe that is designed to measure the absolute electron density in a uniform plasma by recording the resonant frequencies of the reflected signal. The impedance probe built will use a unique surface-mounted dipole antenna to measure the required resonant information between the plasma and probe. The ThinSat mission will help determine if small satellites with an impedance payload can provide accurate real-time plasma parameters in a cost effect and low power budget approach. The results learned from the design and testing of the ThinSat will be used to design an upcoming USCGA CubeSat with an expected launch timeframe in late 2021. The USCGA and partners plan to design and build a CubeSat with an impedance probe payload that will operate in a LEO environment.

1.4 Collaborative partners for space weather measurements

Our key collaborator for designing and testing the impedance probe is the NRL. The NRL has been a global leader in impedance probe design and experiments for decades. Currently, the NRL has the Space PlasmA Diagnostic suitE (SPADE) onboard the International Space Station (ISS). SPADE includes an impedance probe that provides spacecraft charging and ambient plasma parameter measurements for the ISS. It consists of a driven biasable dipole and a passive, receiving dipole antenna. SPADE has been operational on the ISS since May 2019 and has two main operational modes. One is to sweep AC frequencies with a constant DC bias voltage. This is similar to how the ThinSat will operate. The second operational mode is to sweep DC bias voltage with constant AC frequency. By sweeping the DC bias SPADE is able to measure additional plasma parameters.

Also onboard the ISS is the Integrated Miniaturized Electrostatic Analyzer (iMESA). iMESA is part of a space weather constellation being designed and built by the Space Physics and Atmospheric Research Center (SPARC) at USAFA (Maldonado et al., 2020). Once completed the space weather constellation will be embedded on four separate DoD small satellites where they will measure several different plasma parameters (Maldonado et al., 2020). The iMESA uses a laminated electrostatic plasma analyzer to measure plasma density, temperature, and spacecraft charging.

1.5 Research Focus and document organization

This research effort has three main phases. First, the physics and engineering required to design, build, and operate an impedance probe will be research. Second, a plasma chamber will be used to test the antenna and impedance probe hardware in a similar plasma environment to LEO. Third, we will collaborate with the SPADE and iMESA teams to understand how to successfully retrieve raw data from a spacecraft and perform data analysis.

The remainder of this document is organized as follows: Chapter II contains the background physics and engineering required to make impedance measurements with a ThinSat. Additionally, it will contain details how an impedance probe is capable of measuring plasma parameters. Chapter III contains research methodology and testing parameters for this project. Chapter IV contains results from testing the antenna and impedance probe. SPADE data will be analyzed and presented. Chapter V lists conclusions and recommendations.

II. Theory and physics behind impedance measuring concept

In this chapter some targeted principles of plasma physics and the impedance measurement concept are explored. The sheaths of a plasma and probe form an equivalent circuit. Measuring the impedance of the equivalent circuit provides resonant frequency information about the plasma and probe. These resonant frequencies can provide accurate real-time measurements of electron temperature and density. Additionally, in this chapter the physics of the highly compact novel dual strap dipole antenna for the impedance probe is discussed.

2.1 Fluid behavior of plasma

When the ions in a plasma move they create charge separation which leads to electric currents. The electric currents produce magnetic fields that will affect distant ions in the plasma. The long distant influence of charged particles combined with local collisional effects define collective behavior. A fundamental property of a plasma is its ability to shield out applied electric potentials (Chen, 2015). This shielding is known as Debye shielding and is defined by $\lambda_D \equiv \left(\frac{\varepsilon_0 KT_e}{ne^2}\right)^{1/2}$ where n is electron density, KT_e is the thermal energy of the electrons, ε_0 is vacuum permittivity, and e is the fundamental charge of an electron. λ_D is known as the Debye length is the shielding distance or sheath thickness.

There are two main models used when working with plasmas. First there is the fluid model which is significantly simpler to work with and describes a much larger percentage of plasmas (Chen, 2015). In the fluid model individual particles are ignored and fluid dynamics can be used to describe the plasma. This enables us to simplify any dependent

variable and treat the plasma as three spatial dimensions rather than six phase space dimensions. Treating the plasma as a single fluid is called magnetohydrodynamics (MHD). The MHD model will fail and require a more complicated approach when a Maxwellian distribution cannot be maintained (Goldston, 1995). This occurs when local collisions occur infrequently enough to maintain control of the plasma. The second model used to describe a plasma is kinetic theory and often used when the simpler MHD model fails. When kinetic theory is used the velocity distribution function $f(x, v, t)$ of each species in the plasma is needed. Kinetic theory is mostly required for low density or collisionless plasmas as explored for this topic. Table 1 below lists the major features of both MHD and kinetic modeling of a plasma. A description of Kinetic theory is presented in Appendix A.

Table 1. Two methods for modeling plasma behavior.

	Magnetohydrodynamics	Kinetic
Description	Single fluid model combines Navier-Stokes and Maxwell equations. Only need four dependent variables.	Track velocity and location of individual plasma particles. Need seven dependent variables. Use Vlasov and Maxwell equations.
Strengths	Easy to solve and simplest of the plasma models.	Captures much more of the plasma particle behavior than the fluid model. Mathematically more complex with less approximations.
Weaknesses	Misses a lot of the plasma properties. Will fail when there are instabilities, infrequent collisions, non-Maxwellian distribution, and several more factors.	Complex and rigorous to solve. Still does not capture everything.
When to use	Collision frequency is sufficient, Maxwellian distribution, or when high detail in not needed.	Low density plasmas, non-Maxwellian distribution, high temperatures, when more detail is needed.

2.2 Electron density calculated from plasma frequency

In a uniform homogeneous plasma, plasma frequency ω_p is one the most fundamental properties in determining electron density by inspecting impedance. In a plasma, electrons get displaced from some equilibrium point with an ion, resulting in a charge separation. This charge separation creates an electric field and both ion and electron undergo a restoring Coulomb force to reestablish equilibrium. The electron being much less massive than the ion will be pulled towards the ion, overshoot, and oscillate about the ion in attempt to find the equilibrium position. This oscillatory motion resembles harmonic oscillator motion known as the plasma's electron frequency,

$$\omega_{pe} = \left(\frac{n_e e^2}{\epsilon_0 m}\right)^{1/2}. \tag{1}$$

Plasma frequency is the key to calculating the electron density through resonant frequency impedance explorations. From Equation 1, if the plasma frequency is known then the electron density n_e can be calculated since the remaining variables are constants. Numerically, Equation 1 can be approximated by,

$$\frac{\omega_{pe}}{2\pi} = f_p \approx 9\sqrt{n_e}, \tag{2}$$

where the electron density n_e is in m^{-3}. This linear relationship provides a relatively straightforward method to measuring the electron density once the plasma frequency is known.

2.3 Plasma Impedance Measurement Concept

Impedance measurements of a plasma is one method used to measure plasma frequency. It has been an active area of research for decades with most work completed

prior to 1980 (Blackwell et al., 2007). With significant increases in computer technology and space access, impedance measurement research for plasma diagnostics has become a much more active area of research. A Radio Frequency (RF) probe immersed in a uniform plasma can make impedance measurements between the probe and the surrounding plasma. This measurement between the impedance of probe's antenna and the impedance of plasma provides information we can use to derive important plasma parameters (Balmain, 1964).

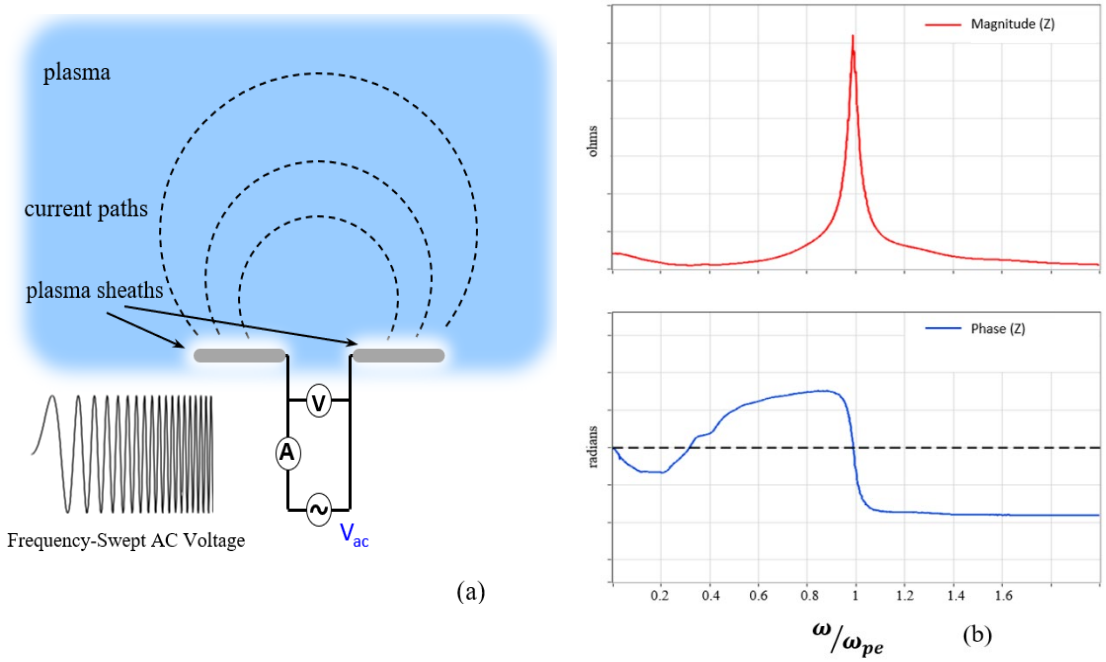

Figure 1. (a) A dipole antenna probe in submerged in plasma with sheath a formed around probe tip. AC voltage sweeps through RF frequencies on the antenna into the plasma. (b) A typical resonant plot with magnitude of the impedance at a maximum and a zero-crossing of the phase. The maximum magnitude occurs at the normalized resonant frequency that matches the plasma frequency.

Both space and laboratory plasma have been investigated with AC impedance measurements using a RF antenna probes (Balmain 1964; Blackwell et al., 2007). Typical impedance probes (IP) emit RF waves swept through a frequency range while measuring the reflected power. The measured reflected power will exhibit resistive behavior between

the plasma and antenna. In an AC circuit paradigm, resistive behavior is impedance and contains both magnitude and phase information as a complex variable. Repeatedly sweeping through a frequency range will generate an impedance spectrum between the probe's antenna and surrounding plasma. Impedance measured as a function of frequency will have resonant regions that characterize the plasma frequency (Patra and Spencer, 2013). At these resonant frequencies, the probe is in resonance with the plasma and the reflected power will be at either maximum or minimum. Figure 1 shows an idealized impedance measurement where the resonant frequencies occur when the phase or imaginary part of the impedance goes to zero. The zero crossing of the phase means the impedance is entirely real and is indictive of a resonant frequency.

Originally it was assumed that IP resonance occurred at the electron frequency of the plasma under inspection. It was not until 1963 when Levitskii and Shashurin (1963) demonstrated that resonance was actually between the plasma and a sheath that forms around the antenna (Ku et al., 1998). Leviskii and Shashurin introduced an equivalent circuit similar to the one shown in Figure 2 to represent the plasma-sheath system. It has been shown that treating the plasma-sheath system as an equivalent resistor, inductor, and capacitor (RLC) circuit provides a decent approximation of the plasma impedance (Blackwell, et al., 2015).

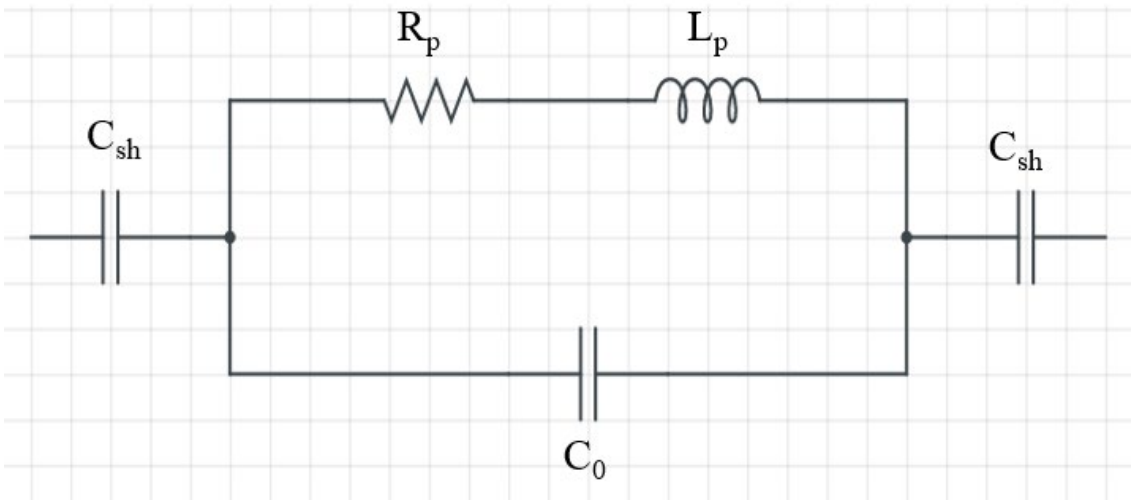

Figure 2. Equivalent circuit model of a plasma and RF probe. C_{sh} is the sheath capacitance, C_0 is the vacuum capacitance, L_p and R_p are the inductance and resistance of the plasma. Inside a plasma chamber a second C_{sh} forms between chamber wall and plasma.

Resonant frequencies are derived by treating the plasma-sheath system as equivalent parallel and series circuit. A sheath will form around the antenna surface when the electrical potential between the antenna and plasma differs. The impedance of the sheath is almost entirely capacitive, and this capacitance can be used to express the total impedance of the sheath (Blackwell et al., 2005). From Figure 2 the plasma and antenna equivalent circuit components that represent the circuit are the sheath capacitance C_{sh} in series with a tank circuit. The tank circuit or LC circuit contains the plasma resistance R_P and inductance L_P, and the initial vacuum capacitance C_0. Series resonance occurs when the frequency is matched for the two sheaths of the equivalent circuit, producing a maximum amount of transmitted energy deposited into the plasma. This series frequency (positioned below the plasma frequency, ω_p) behaves inductively. Consequently, the maximum energy transmission is represented by a minimum in the impedance magnitude which can be observed and compared to its phase (Ku et al., 1998). Parallel resonance,

where transmitted and plasma frequencies are equal, occurs when the capacitance and inductance of the plasma resonate together (Bilen et al., 1999) where the capacitive reactance is $X_C = {}^{1}/_{\omega C}$ and inductive reactance is $X_L = \omega L$ respectively. Parallel resonance is straightforward to determine once an impedance spectrum for the swept frequency range is produced. When a tank circuit is in resonance, the inductor and capacitor on opposite sides of the circuit are equal and opposite. They will cancel each other out to minimize the current deposited into the plasma and drive the impedance to a maximum. A minimum in the impedance (series resonance) closely followed by a maximum (parallel resonance) over a swept frequency range, directly determines the plasma frequency via transmitted frequency equivalence.

Deriving the relationship between the two resonant frequencies and the plasma frequency begins with the equivalent circuit in Figure 2. The expected impedance spectrum of a probe in an unmagnetized plasma can be visualized as the tank circuit previously mentioned with C_{sh} as the sheath capacitance created between the plasma and the vacuum chamber walls (Blackwell et al., 2005). For a spherical capacitor example with radius ρ, in a uniform cold collisionless plasma, and plasma potential of V_P has a capacitance of

$$C = 4\pi\varepsilon_0\varepsilon_r\rho, \tag{3}$$

where the relative permittivity

$$\varepsilon_r = 1 - \frac{\omega_{pe}^2}{\omega(\omega - j\upsilon)}, \tag{4}$$

ε_0 is the vacuum permittivity, and υ is the collision frequency (Blackwell et al., 2005). Permittivity describes how easily a dielectric will become polarized by introducing an electric field. Since this is a RF driven antenna, the circuit model dictates the polarization

is best described as a relative measurement in this case. Other aspects of the plasma represented as circuit elements are,

$$C_0 = 4\pi\varepsilon_0\rho, \tag{5}$$

$$L_p = \omega_{pe}^{-2} C_0^{-1}, \tag{6}$$

$$R_p = \upsilon L_p, \tag{7}$$

where, as previously stated, C_0 is the vacuum capacitance, L_p is the plasma inductance, and R_p is the plasma resistance. For an alternating current electrical impedance Z is the measurement of the magnitude and phase of the resistive nature of a circuit. For a direct current there is only magnitude called resistance. Impedance has units in Ohms (Ω) and its three RLC components are expressed as,

$$Z_R = R, \quad Z_{C_0} = \frac{1}{j\omega C_0}, \quad Z_{C_{sh}} = \frac{1}{j\omega C_{sh}}, \quad Z_L = j\omega L, \tag{8}$$

where $j\omega$ is the complex frequency. Combining the elements of the equivalent circuit found in Figure 2 and Equation 8 in series and parallel, the total impedance of the probe and plasma can be expressed as,

$$Z = \frac{1}{j\omega C_{sh}} + \frac{1}{j\omega C_0 + \dfrac{1}{R_p + j\omega L_p}}. \tag{9}$$

Now by substituting in the values for L_p and R_p Equation 9 can be written as,

$$Z = \frac{1}{j\omega C_{sh}} + \frac{1}{j\omega C_0 + \dfrac{1}{\upsilon\omega_{pe}^{-2} C_0^{-1} + j\omega\omega_{pe}^{-2} C_0^{-1}}}. \tag{10}$$

Borrowing the derivation from Blackwell et al., (2005), the real and imaginary impedance can be separated and reduced by introducing $\gamma = {}^{\omega}/_{\omega_{pe}}$ and $\delta = {}^{\nu}/_{\omega_{pe}}$. The solution has two resulting resonance points (series and parallel) for the impedance where the reactance is zero in frequency space,

$$\omega_1 = \omega_{pe}\sqrt{\frac{C_0}{C_{sh} + C_0}}, \tag{11}$$

$$\omega_2 = \omega_{pe}, \tag{12}$$

where ω_1 is the series resonance and ω_2 is the parallel resonance. Additional terms would need to be considered if a magnetic field were to be introduced. Consequently, for simplicity, the external magnetic field was not included since the AFRL plasma chamber's high density helicon mode was exactly the opposite of our sparse space plasma requirement.

Orbits where our impedance probe is expected to operate will have an appreciable magnetic field, on the order of 0.5 Gauss. Without a magnetic field, plasma oscillations follow the description in Section 2.2. A magnetic field will alter the motion of charged particles to create plasma waves either parallel or perpendicular relative to the external field. This changes the behavior of the plasma and alters the resonant frequency for both weakly magnetized plasmas $\omega_{ce} < \omega_{pe}$ and strongly magnetized plasmas $\omega_{ce} > \omega_{pe}$ (Blackwell et al., 2007). With a magnetic field, the resonant frequencies will exist between the cyclotron frequency ω_{ce} and the upper hybrid frequency ω_{uh} in a weakly magnetized plasma. Subsequently, the parallel resonance becomes the upper hybrid frequency

$$\omega_{uh}^2 = \omega_{ce}^2 + \omega_{pe}^2, \tag{13}$$

and the series resonance shifts to $\omega_r^2 = \omega_{ce}^2 + \omega_{sh}^2$, where ω_{sh} is the unmagnetized series resonance (Blackwell et al., 2007).

2.4 Langmuir Probe verifies impedance probe measurements

Langmuir Probes are another important plasma diagnostic tool popular in laboratory and space plasma experiments likely due to their straightforward construction and ability to measure a wide classification of plasmas. A Langmuir probe consists of a bare wire or metal disk electrically biased with a reference electrode and placed in a plasma, to stimulate electron or ion current collection (Merlino, 2007). Plasma parameters are calculated when the probe is inserted into the plasma and potential of the plasma V_p at the probe tip is measured relative to a reference electrode. Care is taken to directly measure the floating potential V_f of the probe, which is not the same as the plasma potential. The potential of an electrically floating probe will increase or decrease as needed to maintain net zero current or equal flux of positive and negative particles (Merlino, 2007).

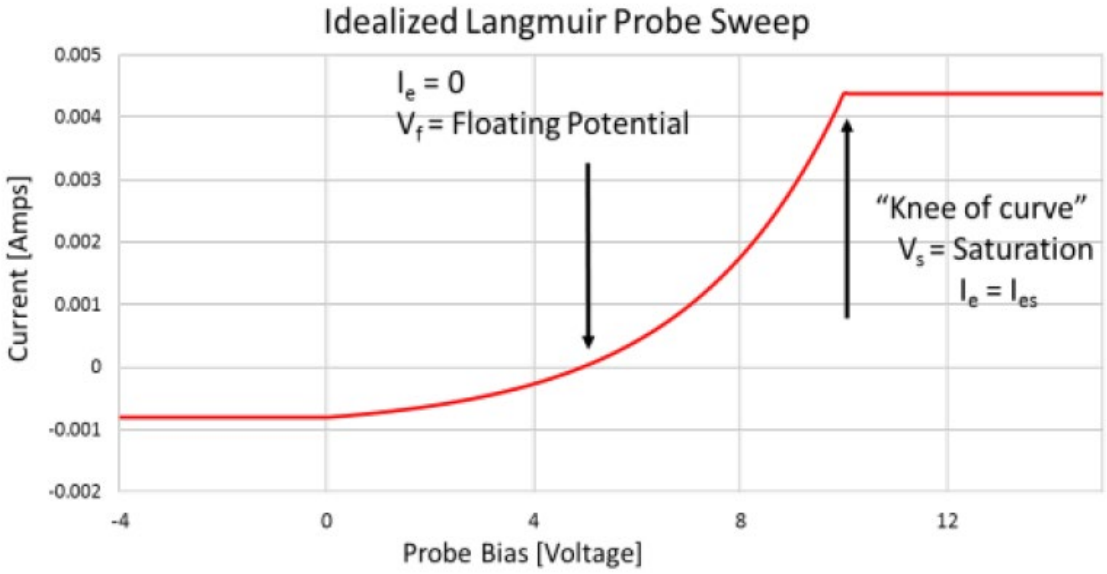

Figure 3. Idealized I-V curve of a Langmuir probe (Zechar, 2017). I_e is electron current, I_{es} is the electron saturation current, V_s is the space or plasma potential, and the "knee of curve" is when the electrons stop being repelled by a negative potential.

As previously mentioned, electrons have smaller masses and much greater thermal speeds than positive ions. Despite electrons and ions in plasma having relatively the same density, the faster electrons will reach the floating probe first (Merlino, 2007). Since a floating potential has zero net current, the probe will float to a negative potential less than the plasma's potential. V_p will be slightly positive due to the faster electrons escaping to the walls of the plasma chamber, leaving a net positive charge. Understanding and resolving the differences between V_p and V_f is done by measuring the current-voltage (I-V) of the Langmuir probe as we apply a bias voltage V_B (Chen, 2003). The V_B is swept from negative to positive voltage and the I-V characteristics of a plasma provide measurements of the plasma parameters. The curve in Figure 3 is described by the equation

$$I_e = I_{es} exp\left[\frac{e(V_p - V_s)}{KT_e}\right], \tag{14}$$

with

$$\mathrm{I}_{es} = en_e A\left(\frac{KT_e}{2\pi m}\right)^{1/2}. \tag{15}$$

Here I_{es} is the electron saturation current, m is the electron mass, and A is the area of the probe tip submerged in the plasma. The electron temperature T_e is obtained by taking the inverse slope of the curve in Figure 3. Once the temperature is known Equation 15 is used to solve for the electron density n_e.

2.5 Additional Plasma Parameters

Electron temperature is the measurement of the kinetic energy in a plasma. It is an important plasma parameter that determines the type of collisions and reactions that can occur and is often inversely related to electron density. Temperature is the indicator used as a threshold to determine the fluid or magnetohydrodynamic (MHD) to kinetic theory plasma description. To measure electron temperature our impedance probe would need an onboard direct current (DC) source (James et al., 2020). Having a DC source enables a probe to bias its sheath relative to the plasma. An onboard DC source will not be used for these impedance probe experiments but will be included in the CubeSat's sensor payload. Once the probe is immersed in a plasma, a sheath will form around the antenna. The sheath will either be electron rich or depleted of electrons depending on the plasma potential between the probe and the background plasma. If the probe is negatively biased compared to the plasma then a depleted electron (ion) sheath will form with a thickness of $S(\phi) =$

$\left(2.5 - 1.87e^{\left(-0.39\frac{\rho}{\lambda_D}\right)}\right)\left(\frac{e\phi}{KT_e}\right)^{\frac{2}{5}}\lambda_D$ (Blackwell et al., 2005). S(ϕ) is a modified form of the Child-Langmuir Law where ϕ is the sheath thickness as a function of the electric potential, ρ is the sphere's radius, and λ_D is the Debye Length.

2.6 ThinSat frame with Short Dipole Antenna

NRL's SPADE sensor was the basis for the design of the IP built for this research effort. We have devised a much more compact version of the SPADE and will use an innovative surface-mounted dipole antenna to provide the required plasma sheath and resonance information. Preliminary research suggests that this is the first ever dual-strap dipole antenna impedance probe successfully tested in the laboratory or deployed into space. The probe will determine plasma density from the resonant impedance frequencies from the gathered phase data described in section 2.3. In the spacecraft sensor framework, impedance probe measurements will be converted from analog to digital and transmitted from low earth orbit (LEO) to a ground terminal via the ThinSat bus.

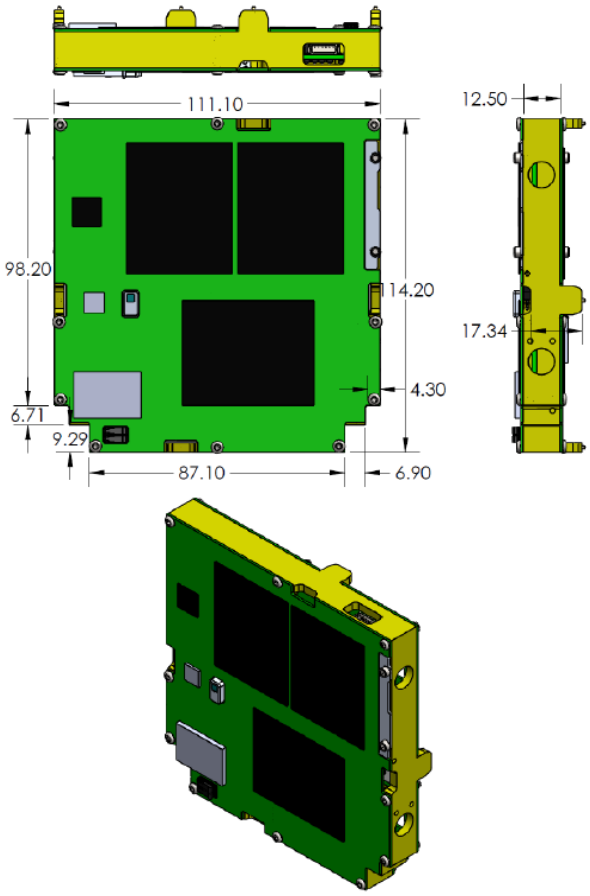

Figure 4. Cartoon of ThinSat frame with dimensions in millimeters. The antennas will attach the yellow section and all electronics must fit inside the case.

A ThinSat is a compact small satellite that requires specific modifications from other space-based impedance probes due to a small size, minimal power budget, and surface mounted dipole antenna configuration requirements. The IP onboard the ThinSat will make measurements of the antenna and ionospheric plasma system impedance, which has two resonant points, at the sheath resonance and at the upper hybrid frequency.

The shape of the antenna plays a key role in the behavior of how the plasma interacts with the impedance probe and has been extensively studied for several decades (Ward et al., 2005). The ThinSat IP will include an electrically short dipole antenna. An

electrically short antenna means the physical dimensions of the antenna are small compared to the free space wavelength at the operating frequency (Ward et al., 2005). A short antenna has several advantages over a long antenna and most research is focused on the short region (Blackwell et al., 2007). Calculating impedance of a dipole antenna begins with the integral $Z = \int_S \bar{J} \cdot \bar{E} dS$, where S is the antenna surface, $\bar{J}$ is the surface current on the antenna, and $\bar{E}$ is the electric field at the surface if the antenna is removed (Balmain, 1964). It is a mathematically complex process to solve for the impedance of a short dipole antenna. The most often cited and complete solution for the impedance of a short dipole antenna comes from Balmain (Balmain, 1964). After the derivation from Balmain's paper the analytical expression for the impedance of a short cylindrical dipole antenna in a magnetized plasma is,

$$\mathrm{Z_{tot}} = \mathrm{Z_{sh}} + \mathrm{Z_p}, \tag{16}$$

where $\mathrm{Z_{sh}}$ is the sheath impedance and $\mathrm{Z_p}$ is the bulk plasma region impedance. The sheath and plasma impedance can be written as,

$$Z_{sh} = \frac{F\left(\beta = \frac{r}{L}\right)}{i\pi\omega\epsilon_0 L} - \frac{F\left(\beta = \frac{r+S}{L}\right)}{i\pi\omega\epsilon_0 L}, \tag{17}$$

$$Z_p = \frac{\sqrt{K'/K_0}}{i\omega 2\pi\epsilon_0 K' L}\left[log\frac{L}{r} - 1 - log\frac{\sqrt{K'/K_0}+1}{2}\right], \tag{18}$$

where r and L are the radius and length of one antenna element. K' and K_0 are elements in the relative permittivity matrix and contain multiple variables which can be found in the 1964 Balmain paper. Balmain's derivation is for a cylindrical dipole antenna while the ThinSat will feature a flat rectangular antenna. Fortunately, the rectangular antenna can be

approximated using Balmain's derivation simply by changing the radius to the width of the antenna. From the sheath impedance in Equation 17 the cylindrical radius of the antenna r is converted to rectangular width $W = 2 * r$. Simply multiplying the radius by two provides a close enough approximation needed to accurately use Balmain's derivation.

III. Engineering and Testing the Impedance Probe

In this chapter the engineering process for the impedance probe throughout this research effort is discussed. It covers the hardware and electronics used to test the antenna and impedance probe. Also covered is the experimental setup for testing the hardware in a plasma chamber using a network analyzer. The calibration process to eliminate stray capacitance from our system will be covered.

3.1 ThinSat Bus

The ThinSat that contains the IP was supposed to launch on the next Antares NG-15 mission. The roughly 10 cm x 10 cm x 2 cm payload platform is modified from the ThinSat platform provided by Virginia Commercial Space Flight Authority (Virginia Space) through a partnership with the USCGA. The mission was going to be launched by Virginia Space at the Mid-Atlantic Regional Spaceport (MARS). Unfortunately, due to engineering setbacks our payload will not be ready for launch. However, the USCGA and Virginia Space partnership will continue with a CubeSat launch in late 2021. The CubeSat will contain all the hardware of the ThinSat IP as a key part of its payload.

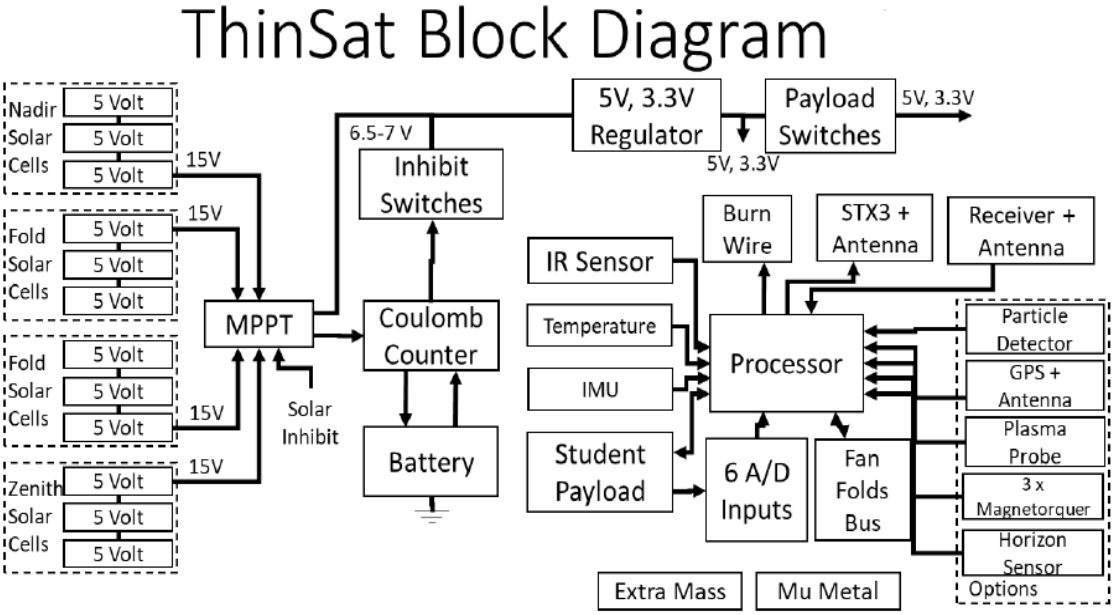

Figure 5. Image of ThinSat bus block diagram.

VaSpace includes a standard bus for all ThinSats so power, telemetry and communications are provided through it (James et al., 2020). ThinSats are designed to use a sensor board. This board connects to the bus and captures light intensity, temperature, and pressure. The data is communicated through the bus, packetized, and broadcast back to Earth over the 5-day life of the ThinSat mission (James et al., 2020). The IP connects into the bus using the same connector as the Twiggs Spacelab Primary Board (TSLBD) circuit board. The connector is surface-mounted and snap-fits to the bus. Due to the layout of the ThinSat frame, the bus and sensors are within a few millimeters of each other. A custom cable was designed that enables the connectors to connect the sensor and bus.

3.2 Dual strap dipole antenna design

Using impedance matching to determine electron density in a plasma is not a new concept and has been an active area of research for several decades. Impedance measurements work by finding resonance of a plasma and a probe antenna. Therefore,

understanding the design and characteristics of the antenna is essential. Due to the size and shape of the ThinSat our team chose to use a dual strap dipole antenna.

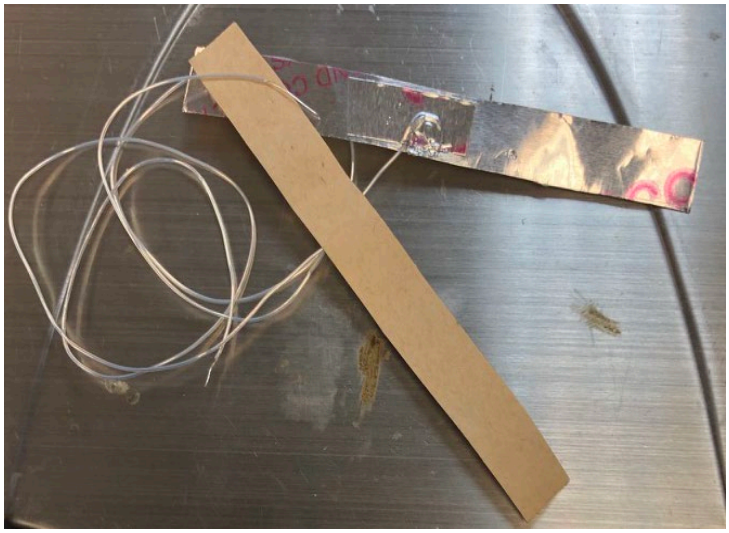

Figure 6. Image of the antenna used to measure impedance. Each antenna is approximately 80 mm x 10 mm x .20 mm. The back section peels off and the adhesive material attaches to the ThinSat frame.

Our payload will be the first ever surface mounted dipole impedance probe to be tested in space when launched on the CubeSat. The ThinSat antenna consists of two strips of aluminum attached to opposite sides as seen in Figure 6. Each antenna is approximately 80 mm x 10 mm x .20 mm. The back on the antenna that attaches to the metallic surface of the ThinSat from Figure 4. The back section is electrically insulated to prevent the entire frame acting as an antenna. Engineering requirements set by VaSpace require any external mounted components to be less than 0.5 mm in thickness. The extra thickness from attaching an antenna on each side of the ThinSat frame is within acceptable limits.

3.3 Experimental setup

Testing of the IP is split into two phases based on their functional sophistication and mission goals. First, the surface mounted antenna design needs to be tested to ensure it operate properly during impedance measurements. Second, the impedance circuit board will be tested on the bench to verify it can make impedance measurements without a network analyzer. Both testing phases are discussed in detail later in this chapter.

Testing the antenna and IP in an environment representative to the ionosphere requires the use of a plasma chamber. We partnered with the Air Force Research Labs (AFRL) Sensor Directorate to use their plasma chamber at Wright Patterson Air Force Base (WPAFB). AFRL has a Kurt Lesker stainless steel cylindrical vacuum chamber to contain the plasma environment. The chamber's dimensions are 100 cm in length by 50 cm in diameter. The chamber has several ports of various sizes which provided us to position our testing equipment as needed. The chamber has an Edwards B723-01-000 vacuum pumping station which contains both a roughing pump and a turbo molecular pump. This vacuum system enables the chamber to achieve pressures as low as 100 nTorr.

Argon gas is used to create the plasma and constant pressure is maintained from the computer terminal. A N9923A FieldFox Handheld Network Analyzer is used to generate the complex impedance spectrum for the antenna test only. Data processing software captures the raw impedance data.

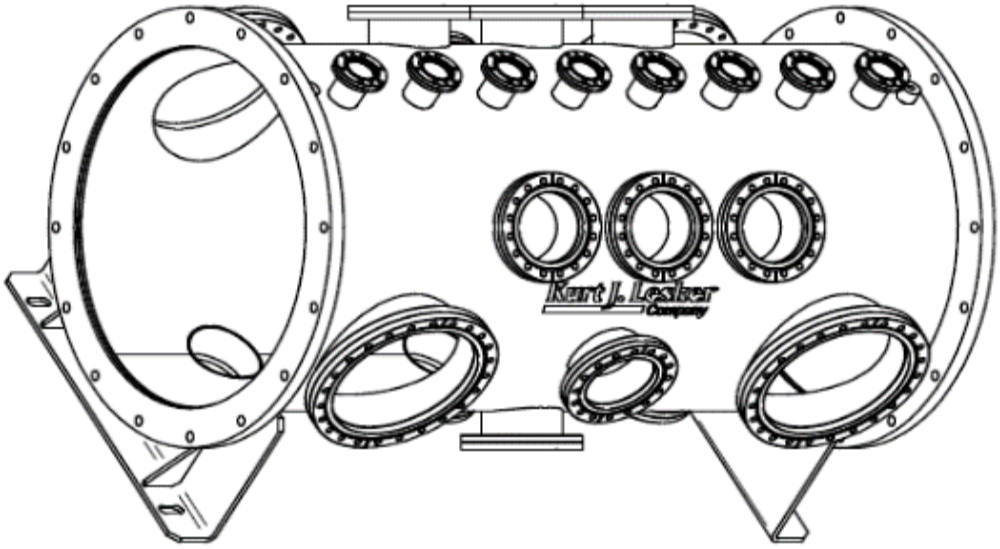

Figure 7. Plasma chamber drawing used to test the surface mounted antenna and impedance probe in a plasma environment.

The plasma chamber uses a 27.12 MHz Helicon plasma source to generate the plasma. Helicon plasma contains neutrals, ionized particles, and a magnetic field. Helicon waves ionize the particles to create the plasma and can achieve both high and low densities (Chen, 2015). The RF noise generated at 27.12 MHz by the helicon heating antenna will be present while the plasma is operating in steady state. To account for this noise, there is a DC block at 27.12 MHz which ignores this frequency. The alternative is to operate in the plasma afterglow which occurs briefly right after the plasma is shut off. The afterglow exists in the millisecond range. The network analyzer is not capable of accepting an external timing trigger which prevented operating in the afterglow due to the lack of proper timing.

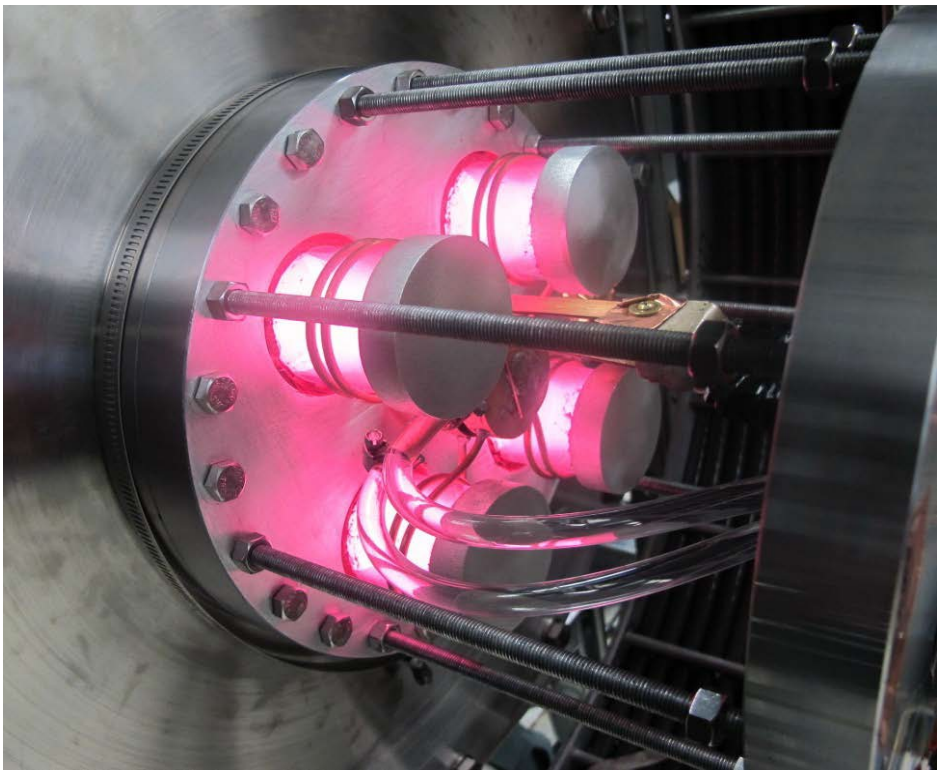

Figure 8. Image of a quad helicon source similar to the one used in the AFRL plasma chamber.

3.4 Generation of magnetic field

To properly explore the environment the impedance probe will operate in, electromagnets are used to generate a magnetic field. Recall from Equation 13 the upper hybrid frequency depends on the cyclotron frequency which is controlled by the background magnetic field. Therefore, the upper hybrid frequency changes as the strength of the magnetic field surrounding the chamber is varied. Electromagnets supply a uniform magnetic field $\overleftrightarrow{B_Z}$ along the axis of the 100 cm chamber. The chamber consists of four coils of electromagnets and was configured by AFRL. Figure 9 below shows the four electromagnets in blue that surround the vacuum chamber.

Figure 9. Cartoon of a plasma chamber with electromagnets surrounding the chamber. The spacing and size of the electromagnets was determined to provide a uniform magnetic field throughout the entire chamber.

3.5 RF I-V measurement technique

Impedance spectrum measured by the RF I-V method is used by our impedance probe circuit board. This method provides better accuracy and can cover a wider impedance range than the reflection coefficient method of a network analyzer (Agilent Handbook, 2013). The impedance probe circuit board completes the RV I-V technique without the need of the network analyzer. The microcontroller is the signal source that generates and sets the output frequency of the RF and local oscillator (LO). It also sets the phase of the LO direct digital synthesizer (DDS), either 0° or 90° relative to the RF DDS which allows us to measure the real and imaginary parts of the current and voltage. The detection transformer picks off the RF voltage (RFV) and RF current (RFI) signals in the circuit and routes them back to the two mixers. Each signal is mixed with the LO signal and low pass filtered. Then the microcontroller sets a new output frequency, and the process repeats until

the frequency sweep is complete. The frequency will continuously sweep over a selected frequency range and output the RFI and RFV measurements to a serial monitor through a mini-USB cable.

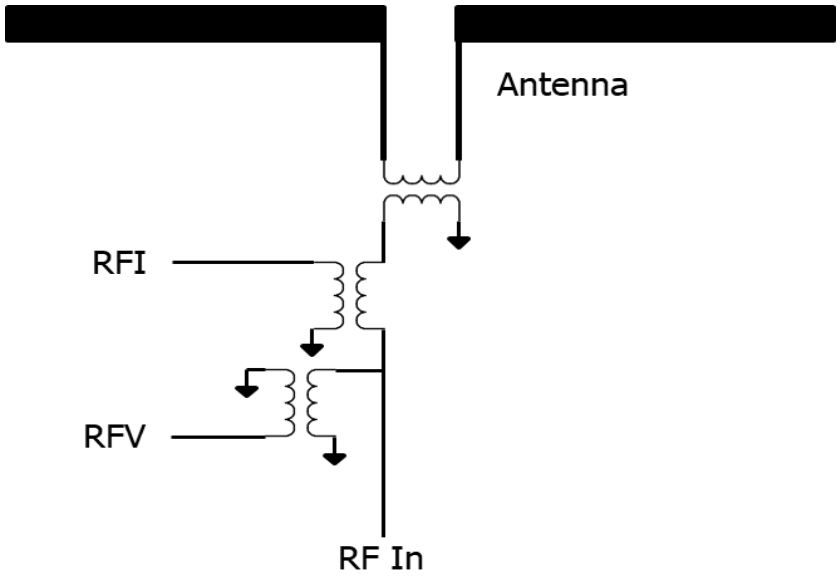

Figure 10. RF-IV dipole antenna schematic that will be used to make impedance measurements. The RFI and RFV impedance matching transformers are 1:1 so the impedances will be equal. We designed the transformers for 50 Ohms and care was taken to have the measurement circuit for RFI and RFV be matched to 50 Ohms. This allows for estimates of the voltage measured at RFI and RFV to be made by replacing the RFI and RFV transformers with 50 Ohm resistors and the antenna transformer can be replaced by the impedance between the plasma and antenna.

The RF-IV measurements are made using a mixer chip that produces the product of the LO signal and the RFV and RFI signal. The output mixer can be written as:

$$X = A\cos(\omega t + a) \times B\cos(\omega t + b)\,, \tag{19}$$

$$X = \frac{AB}{2}[\cos(2\omega t + a + b) + \cos(a - b)], \tag{20}$$

where A is the amplitude of either RFI or RFV, B is the LO amplitude, and a and b are the phase of each signal respectively when they enter the mixer. The output of the mixer is low pass filtered to remove the $2\omega t$ term. Remaining is the DC component that is proportional to the amplitude of the RFI or RFV and its phase relative to the LO. This DC value is recorded by the Analog-to-Digital Convertor (ADC). Because this output could be bipolar and the ADCs on the ThinSat needed unidirectional signals, there is a circuit to invert the signal if it is negative. The appropriate sign needs to be reintroduced to the measured amplitudes. Assuming the signs are fixed, we can write $X_0 = \frac{AB}{2}\cos(a-b)$ and $X_{90} = \frac{AB}{2}\sin(a-b)$. The LO is set to 90 degrees phase which can also be written compactly in complex notation:

$$X = X_0 + iX_{90} = \frac{AB}{2}e^{i(a-b)} \tag{21}$$

Since X represents either RFI or RFV and it is expected that the LO amplitude and phase to be the same for both, the impedance of a given frequency can be express as,

$$Z = \frac{RFV}{RFI} = \frac{A_{rfv}}{A_{rfi}}e^{i(a_{rfv}-a_{rfi})}. \tag{22}$$

We repeat this process for each frequency to generate the complex, uncalibrated impedance spectrum.

3.6 Impedance probe custom circuit board

The impedance probe will produce both AC and DC voltages and currents through an Arduino Pro Mini. While the impedance probe components can produce and transmit positive and negative voltages and currents, the Arduino Pro Mini is not capable of reading negative voltages and currents. Reading a negative voltage or current can damage the ADC

on the Arduino and potentially damage the AT328MEGA processor in the Arduino. Since the Arduino is mission-critical, eliminating potential problems is necessary.

To eliminate this problem, we created a subcircuit using comparators, invertors and multiplexers. This subcircuit compares the output of the AD9834 to Ground and inverts the output. If the output of the AD9834 is less than Ground, then the inverted output is passed through a 2:1 Multiplexer to the Arduino. If the output of the AD9834 is positive, it is passed through the 2:1 Multiplexer to the Arduino. The Comparator and Inverters are built using LM398 Operational Amplifiers (Op Amps). The initial tests were done with LM741 Op Amps. The LM741 is a general-purpose Op Amp that has heavy use in designs. This Op Amp needs 5 V to operate. Since the Impedance Probe operates at 3.3 V, the LM741 would require a 5 V line to it, or a Voltage Divider would be necessary to provide 3.3 V to the rest of the IP. The LM398n is a low power Op Amp that operates at 3.3 V. The LM398n, in testing, proved to be a better choice. A single dual dip LM398n package provides two Op Amps which are required to create the Comparator and Invertor for the subcircuit, required for each output.

As the AD9834 DDS is a signal generator. As the DDS-generated signal interacts with the Plasma, the response is received by the antenna. The 1:1 transformers are used to measure the current and voltage of the signal response. Using 1:1 transformers will attenuate transient noise with very little signal loss. With voltage limitations in the processor, it becomes very important to limit losses in transforming signal current to voltage.

Biasing the signal presented an interesting challenge. The acceptable input voltage range for the Arduino Pro Mini is 0 – 3.3 V. We can correct for the voltage bias with a

series capacitor. While this reduces the output voltage, it can be mapped to a higher known value.

3.7 Antenna test with Network Analyzer

The first test conducted in the plasma chamber was verifying the functionality of the dual strap antenna. The antenna was tested to see if it is capable of operating in a plasma environment similar to the ionosphere. The device tested consists of a dual-strap antenna surface mounted to a ThinSat frame connected to a network analyzer, through a transformer. Figure 11 contains a cartoon of the antenna device and hardware used for this test. The network analyzer produces the frequency sweep, transmits the RF signal through an SMA cable to the antenna device, and measures the reflection coefficient. Few electronic components are used for this test in order to minimize sources of error to generate an impedance spectrum. The antenna device connects to the network analyzer via a rigid SMA feedthrough into the plasma chamber. The antenna connects to the transformer through a SMB-mini connector. For the calibration process the antennas are disconnected and replaced with custom made calibration standards to measure the standard resistance, capacitance, and inductance. The calibration process is explained in Section 3.8.

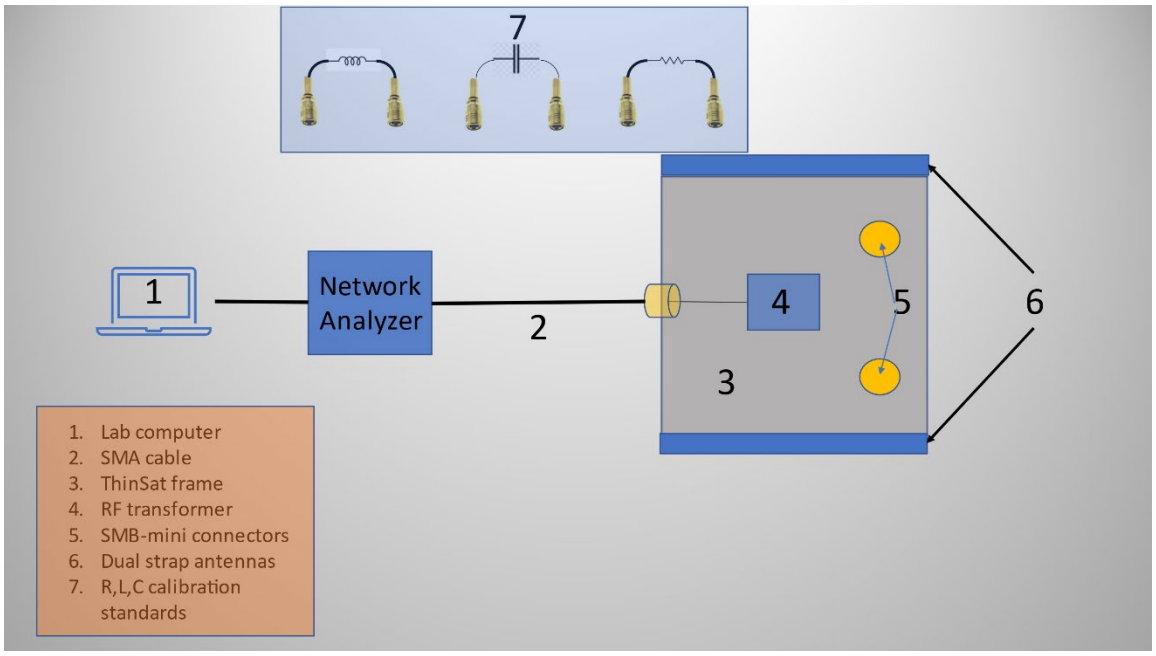

Figure 11. Cartoon of antenna attached to the ThinSat frame, network analyzer, and calibration standards needed to test the antenna. The lab computer (1) initiates the network analyzer to measure the impedance. The calibration standards (7) individually plug into the SMB-mini connectors (5) for the calibration process only. After calibration, the antennas (6) plug into the SMB-mini connectors (5) while measuring impedance.

Before testing the antenna, the network analyzer must be calibrated to exclude all impedances of all cables. This way the network analyzer will ignore everything up the SMA connector where we attach our antenna. The next step is to verify that the antenna deposits power in a plasma as the AC frequency is swept. A 3D printed plastic ThinSat frame with the 80 mm x 10 mm antennas fixed to the sides of the frame was used for this test. Figure 12 contains a sideview image of the ThinSat frame with the dimensions of the frame and antenna.

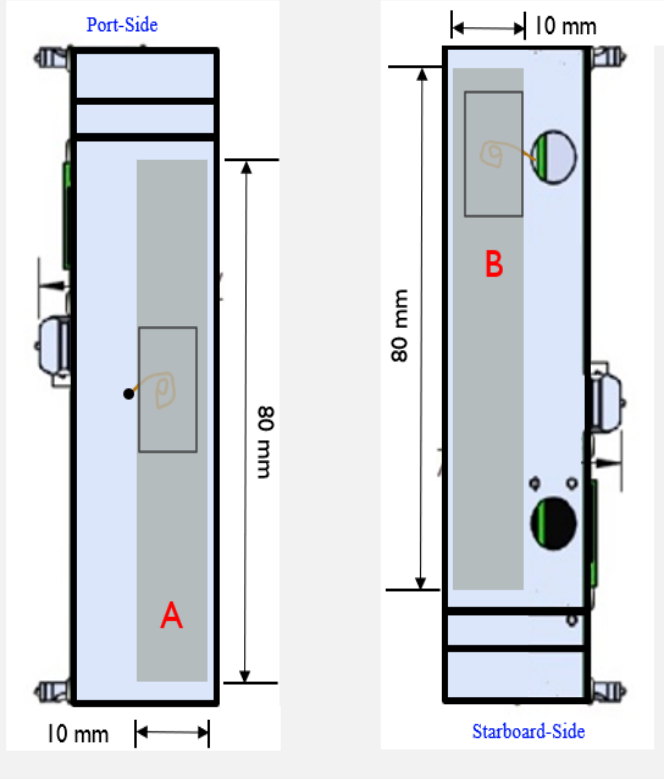

Figure 12. Side view of ThinSat where the antenna will attach. The wire from the antenna is curled to increase its surface area. This reduces the chance of the antenna being pulled out.

The antennas were each connected to a mini-SMB connector that were wired to a transformer. An SMA bulkhead was attached to the ThinSat frame and wired to a surface mount RF transformer. Inside the plasma chamber the ThinSat antenna device is attached to a rigid SMA cable with the antennas oriented parallel to the plasma stream. The SMA cable connects via a feedthrough to the network analyzer. The network analyzer was connected in an S_{11} configuration where it swept the desired frequency range and measured the complex reflection coefficient Γ,

$$\Gamma = \frac{Z - Z_0}{Z + Z_0}. \tag{23}$$

After verifying the antenna was depositing power by observing a decrease in the reflected signal during frequency sweeps, the device was tested in a plasma by closing the chamber and pumping pressure down to a few millitorr of pressure. Then the Argon gas is pumped in at a steady flow to maintain a desired pressure. The pressure can be adjusted from the lab computer between each data set. Next the plasma is turned on and the network analyzer is triggered from the lab computer to sweep a frequency range and measure the reflection coefficient. After each experimental run the magnetic field, chamber pressure, and voltage used to trigger the plasma were varied to try and produce resonant frequencies within our frequency range. Increasing the RF power in the chamber causes more neutrals to ionize which produces a more dense plasma. Increasing the magnetic field creates a more tightly focused plasma stream as the plasma particles orbit around the magnetic field lines. Increasing the chamber pressure increases the neutral particle density. This provides more particles to ionize when the plasma ignites as well as more neutrals for the ions to collide with. A high collision rate inside the chamber may prevent the plasma from reaching the back of the chamber where our antenna device is placed. Decreasing the collision rate should have the opposite effect. Once a resonant frequency is observed, simply adjusting the RF power level should result in the resonant frequency shifting. Less RF power produces less plasma and the resonant frequency should drop. Increasing the RF power produces more plasma and the resonant frequency should increase. This understanding is used to verify correct observations of an impedance spectrum as the RF power is adjusted.

3.8 Impedance Probe Calibration

One of the most important steps to the testing phase is the calibration procedure. Calibration attempts to account for the effects of all the parasitic impedances in the circuit,

leaving only effects beyond the calibration plane. The process we used was borrowed from the four terminal circuit model in the Agilent Impedance Measurement Handbook.

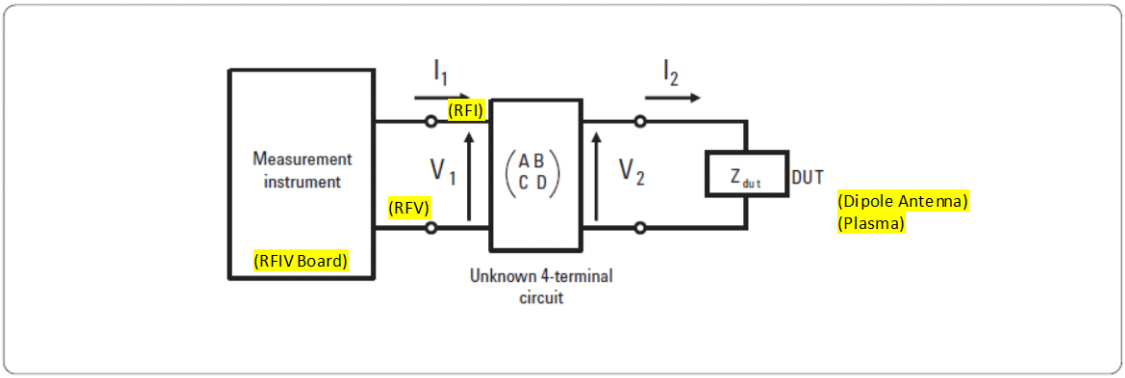

Figure 13. 4-terminal circuit from the Agilent Impedance Measurement Handbook (Agilent Technologies, 2013).

The four terminal circuit model is the same as the open/short/load compensation and is expressed by the following matrix equation, $\begin{pmatrix} V_1 \\ I_1 \end{pmatrix} = \begin{pmatrix} A & B \\ C & D \end{pmatrix} \begin{pmatrix} V_2 \\ I_2 \end{pmatrix}$, where we need to solve for V_2 and I_2 after measuring V_1 and I_1. Multiplying the matrix equation and solving for impedance we get,

$$Z_{meas} = \frac{V_1}{I_1} = \frac{AV_2 + BI_2}{CV_2 + DI_2} \tag{24}$$

where Z_{meas} is the measured impedance of the device under test (DUT), and the true value of the DUT is,

$$Z_{DUT} = \frac{V_2}{I_2} \tag{25}$$

The number of unknown coefficients can be reduced from four to three by factoring out DI_2 from Equation 25,

$$Z_{meas} = \frac{V_1}{I_1} = \frac{DI_2}{DI_2}\frac{{}^{A}/_{D}\,{}^{V_2}/_{I_2} + {}^{B}/_{D}}{{}^{C}/_{D}\,{}^{V_2}/_{I_2} + 1} = \frac{A'Z_{DUT}+B'}{C'Z_{DUT}+1} \tag{26}$$

Manipulating Z_{meas} to Equation 26 leads to the expression for the measured impedance as a function of three coefficients of the model circuit and the actual Z_{DUT}. Three standards are required to determine the three unknown coefficients. Writing the three equations, where Z_{mi} is the measured impedance of the i-th standard Z_{si},

$$\begin{aligned} Z_{s1}A' + B' - Z_{m1}Z_{s1}C' &= Z_{m1} \\ Z_{s2}A' + B' - Z_{m2}Z_{s2}C' &= Z_{m2} \\ Z_{s3}A' + B' - Z_{m3}Z_{s3}C' &= Z_{m3} \end{aligned} \tag{27}$$

Next a solution is needed for the system of equations for A', B', and C'. Solving the top equation and substituting for these coefficients, expression for the calibrated measurement is:

$$Z_{DUT} = \frac{Z_{meas}-B'}{A'-C'Z_{meas}}. \tag{28}$$

To implement the calibration process, either calibration standards Z_{si} that would be well represented by the ideal measurements are chosen or measure their impedance as a function of frequency on a calibrated network analyzer. Next, measure the impedance Z_{mi} of the three standards (resistor, capacitor, and inductor) using the IP board over the same frequency range. With Z_{si} and Z_{mi} calculate the calibration coefficients A', B', and C' in Equation 27 for each frequency. Once the calibration coefficients are calculated measure two tank circuits whose values are chosen to place the resonant frequency in the low and

high end of our sweep range with the impedance probe board. Lastly, we calculate the calibrated impedance using Equation 28 for Z_{DUT} and the calculate calibration coefficients.

3.9 Impedance Circuit Board Test

To test the impedance probe circuit board, the experimental setup was adjusted. The goal is to see if the custom-made circuit board is capable of replacing the network analyzer and produce an impedance spectrum. The IP circuit board is attached to a ThinSat frame with the same antenna used in the previous tests. Female SMA connectors are wired to test point one (TP1) and test point two (TP2). TP1 and TP2 connect to the antenna when testing and can be switched to the resistor, capacitor, and inductor calibration standards similar to the previous test. To operate the IP the circuit board is connected to an Arduino programmed to trigger RF I-V measurements in the IP. The Arduino is connected via USB-mini to a computer that provides power and performs as a serial monitor. The Arduino is preprogrammed to initiate the impedance circuit board and pass the data to the serial monitor. The computer records the frequency and RF-IV measurements made by the IP. The raw uncalibrated impedance spectrum undergoes the same calibration process as the previous test.

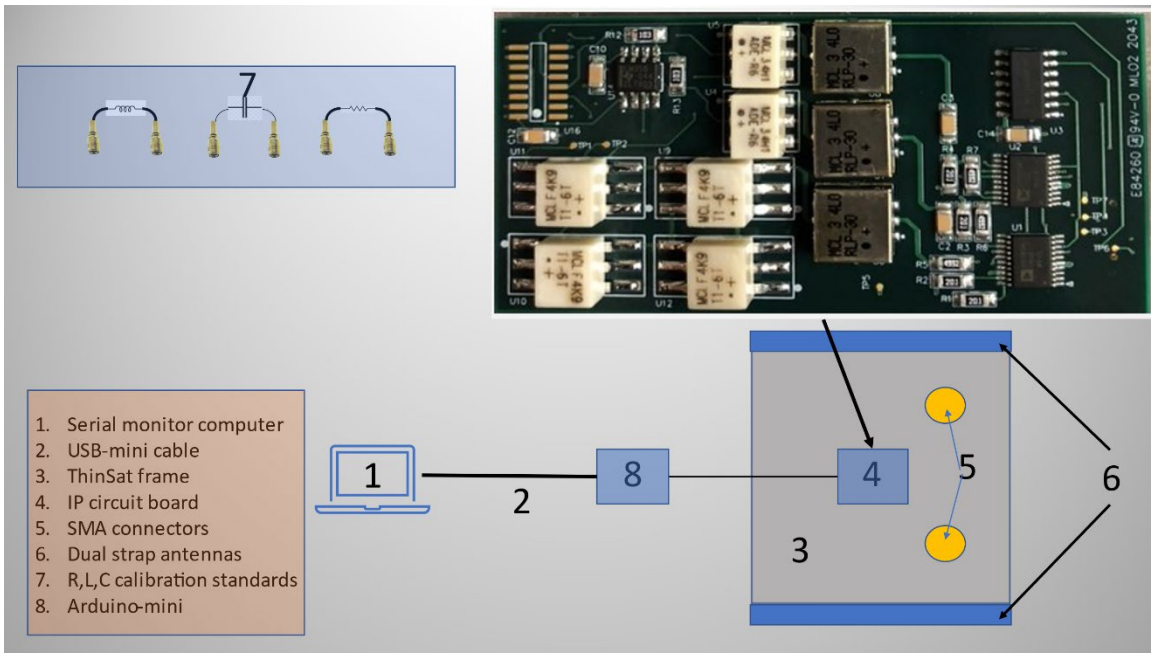

Figure 14. Cartoon of the ThinSat frame, serial monitor, and calibration standards needed to test the impedance probe circuit board attached to the antennas. The Arduino (8) triggers the IP (4) to perform RF-IV measurements. The calibration standards (7) plug into the SMA connectors (5) for the calibration process only. The antennas (6) plug into the connectors (5) while measuring impedance.

First, the IP was tested on the bench to verify the functionality of all hardware prior to using a plasma chamber. Figure 14 contains a schematic of components used to test the IP. The SMB-mini connectors were difficult to use in the previous test and were replaced with SMA connectors. After the bench test verifies that we can measure RF I-V data from the IP and Arduino the hardware will be tested in the plasma chamber. A USB-mini feedthrough adaptor for the plasma chamber was made. For calibration, the Z_{mi} of the three standards will be individually connected to the SMA connectors and measured. Next the standards will be disconnected and the dual-strap antennas will be attached. The ThinSat will be placed in the plasma chamber and connected to the USB-mini feedthrough. The

plasma chamber will set to similar conditions as the antenna device test. The computer with the serial monitor will trigger the Arduino and begin the frequency sweep.

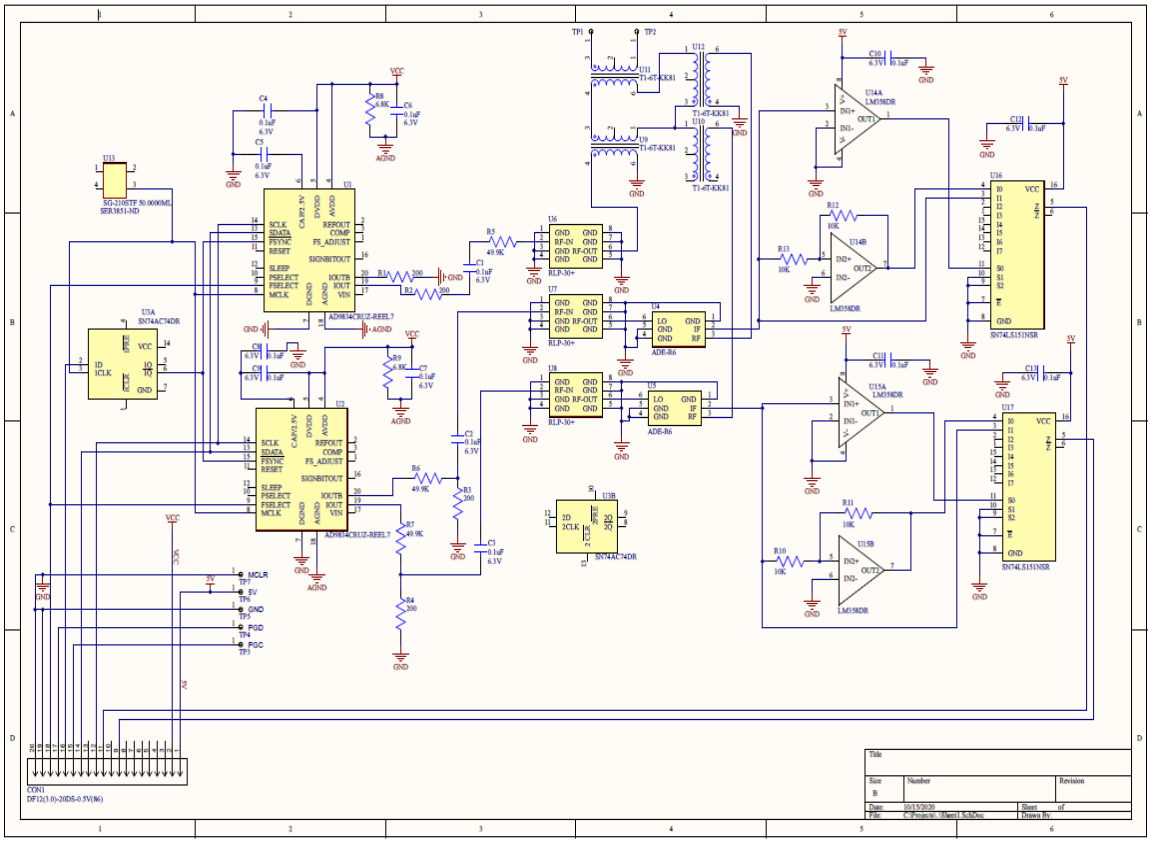

Figure 15. Impedance probe circuit board schematic. The pins located at the bottom left of the schematic is where the Arduino connects to the IP.

3.10 Scaling process for expected ionosphere plasma densities

The AFRL plasma chamber managed to produce plasma densities that are expected in ionosphere where our impedance probe will operate after multiple months of experimenting. According to SPADE data we expect to operate in plasma densities of $n \approx 10^5$ cm^{-3}. However, this density is a couple orders of magnitude lower than what the chamber typically produced. While developing SPADE, the NRL created a scaling process

that attempts to predict the currents that will be measured by an impedance probe during normal operations in the ionosphere. In the interim, values from the scaling process were used to determine the impedance circuit components in order to set the appropriate ranges for these current measurements. The scaling code from the NRL needed only minor adjustments to account for the surface mounted antenna geometry. After converting the scaling code it was determined that the range of frequencies our impedance probe will need to measure is 2 MHz to 10.2 MHz. The expected impedance values within this frequency range varied from $5.0 \times 10^3\ \Omega$ to $7.0 \times 10^7\ \Omega$. Using Ohm's Law with the maximum impedances and the probe's output voltage of 5.5 V, we can estimate the RFI values that we expect to measure while operating in the ionosphere. The minimum and maximum RFI values the probe will need to measure are estimated to be between $0.0785\ \mu A$ and $1000\ \mu A$. An amplifier will likely be needed for the final IP payload in order to measure the lower end of the RFI range. Additionally, due to impedances within the circuit the supplied voltage will be less than 5.5 V. Therefore, we should expect less current than the scaling code estimates.

IV Results

In this chapter the results are provided from testing the antenna and the impedance probe. The details about electronic components used will be discussed. SPADE data from onboard the ISS during operations is also included. The SPADE data will be used to verify our expected plasma densities of the ionosphere.

4.1 Dual strap dipole antenna with network analyzer

Measuring the impedance begins with AFRL python code which triggers the network analyzer. The network analyzer saved the data traces containing the complex impedance over a frequency range we are testing. Raw impedance data from the network analyzer is combined with the calibration standards of the RLC components in the LabVIEW calibration code. The LabVIEW code calculates the calibrated impedance spectrum. The calibrated impedance data is then plotted in MATLAB. After several data runs, it was discovered that 7.5 mTorr of Argon gas was the ideal pressure for creating a weakly ionized plasma over the frequency range selected. Table 2 contains the input values for this experiment.

Table 2. Antenna Test Input Values

Chamber pressure	7.5 mTorr & 5 mTorr
Magnetic field strength	0 G
RF power range	70 W-200 W
Measured resistor	50 Ω
Measured capacitor	1.8 pF
Measured inductor	1 μH
Frequency range	30 MHz – 100 MHz
Number of data points in each frequency sweep	210

The frequency range was selected to begin after 27.12 MHz to avoid the DC block at that frequency and produce noise in our data. The RF power that ionized the gas in the chamber was varied in order to examine a shifting resonant frequency. 70 Watts is the lowest power the plasma chamber could generate while anything greater than 200 Watts put the resonant frequency outside our sweep range. The measured RLC components for calibration and the number of points per sweep were selected due to previous NRL experiments with a similar setup. For our experiment the chamber pressure capable of producing impedance measurements maxed out at 7.5 mTorr. Anything greater was not capable of measuring an impedance spectrum likely due to an excess number of neutrals inside the chamber. All data sets taken in the AFRL plasma chamber contained a spike at 54 MHz. At 54 MHz there is a notch filter to block the second harmonic of the helicon plasma.

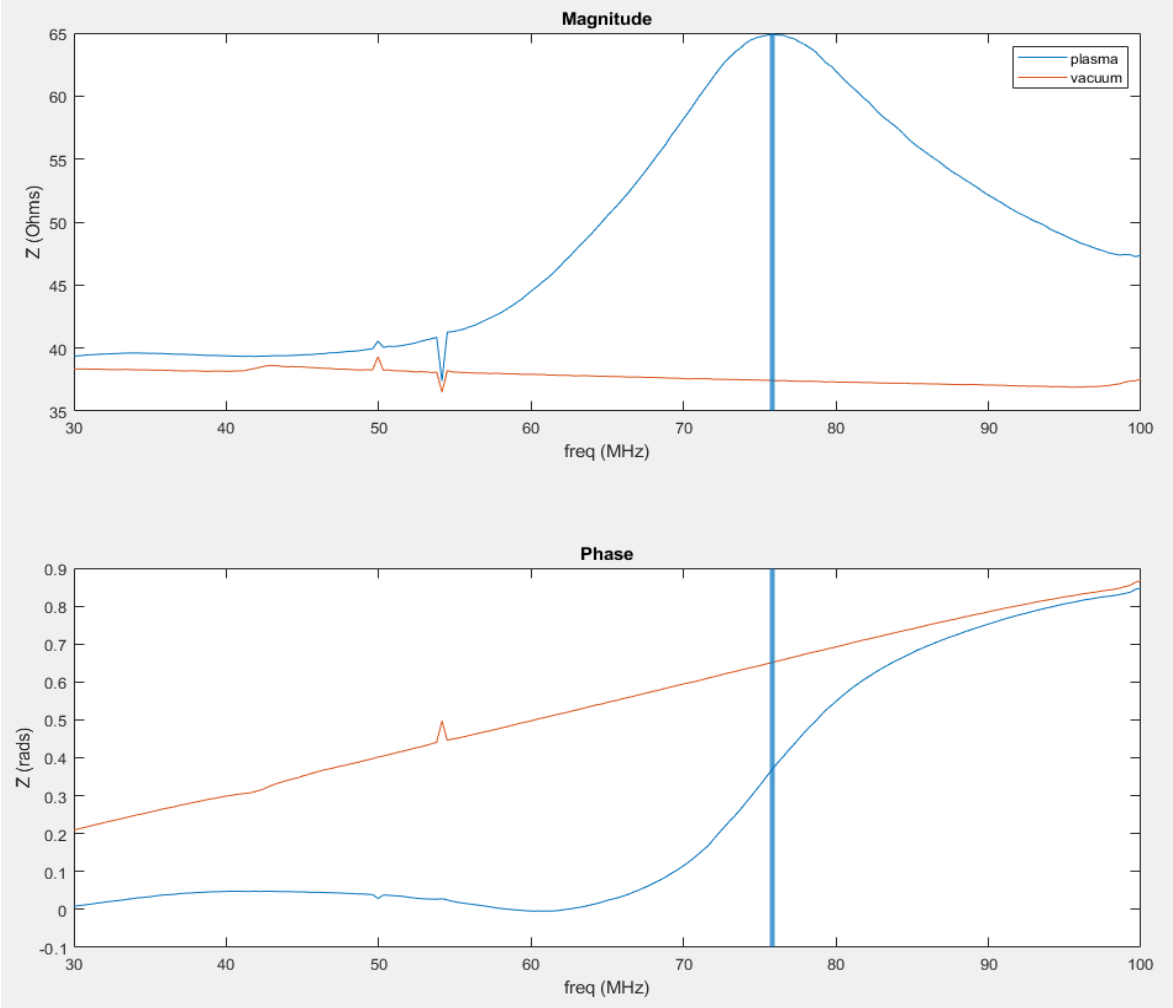

Figure 16. Measured magnitude and phase of the antenna-plasma impedance. The chamber pressure was set to 7.5 mTorr of Argon and the plasma was triggered with 150 W of power. The sharp spike at 54 MHz is from the notch filter.

The vacuum trace is where the plasma is not turned on. With no plasma the vacuum trace measures the free space capacitance of the antenna in parallel with the chamber wall. The plasma impedance in Figure 16 would ideally be the impedance between the plasma and our antenna. However, there will still be extra parasitic capacitance in parallel with the dipole antenna. A decent approximation for the impedance is to subtract off the vacuum impedance from the plasma. This technique was borrowed from the NRL SPADE team.

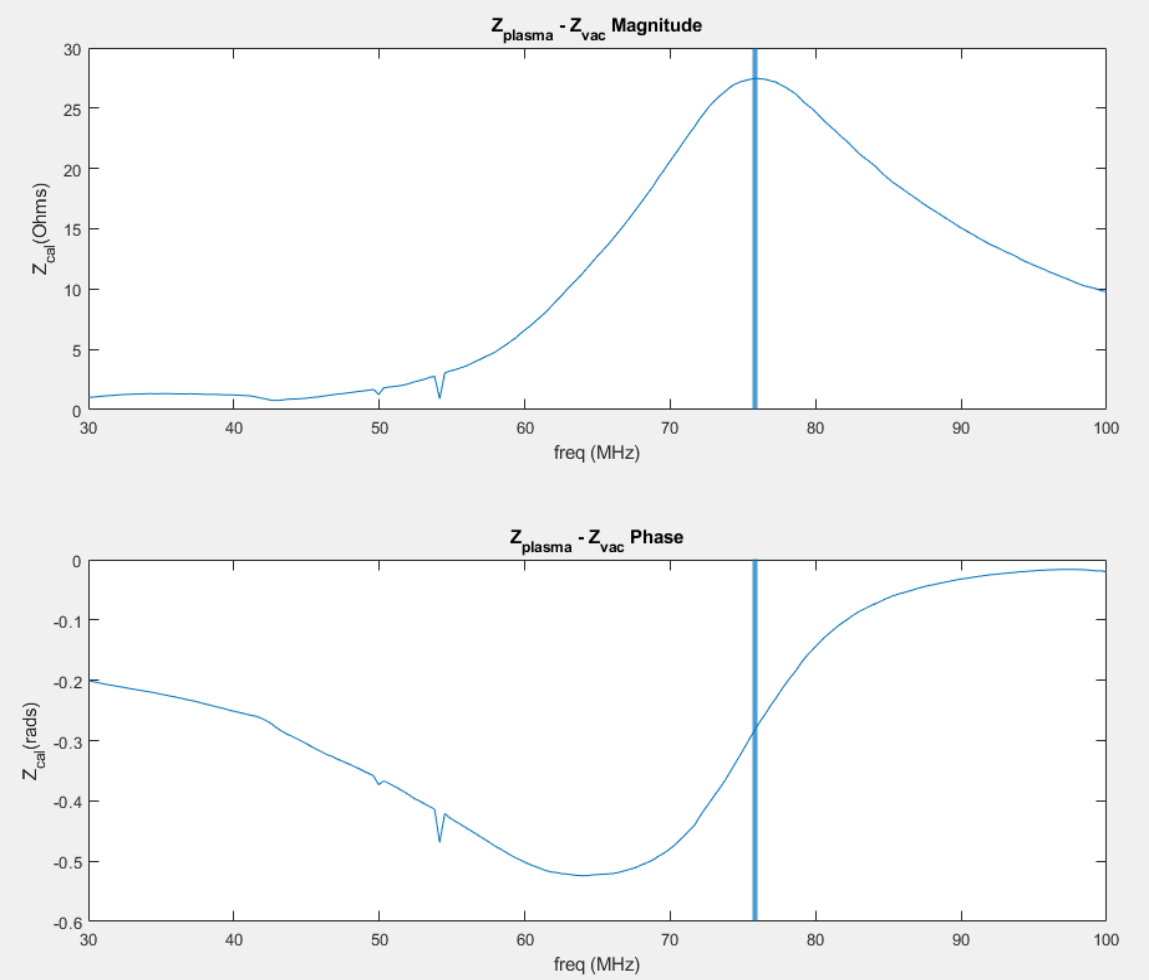

Figure 17. Magnitude and phase of antenna-plasma impedance after calibration. The maximum of the magnitude at 75 MHz is the parallel resonance between the plasma and antenna.

Figure 17 is the calibrated impedance spectrum after subtracting off the vacuum impedance. From the maximum of the magnitude in Figure 17 a parallel resonance of 75 MHz was measured. Using Equation 2 the plasma electron density was calculated to be $n_e = 7.1 \times 10^7 cm^{-3}$.

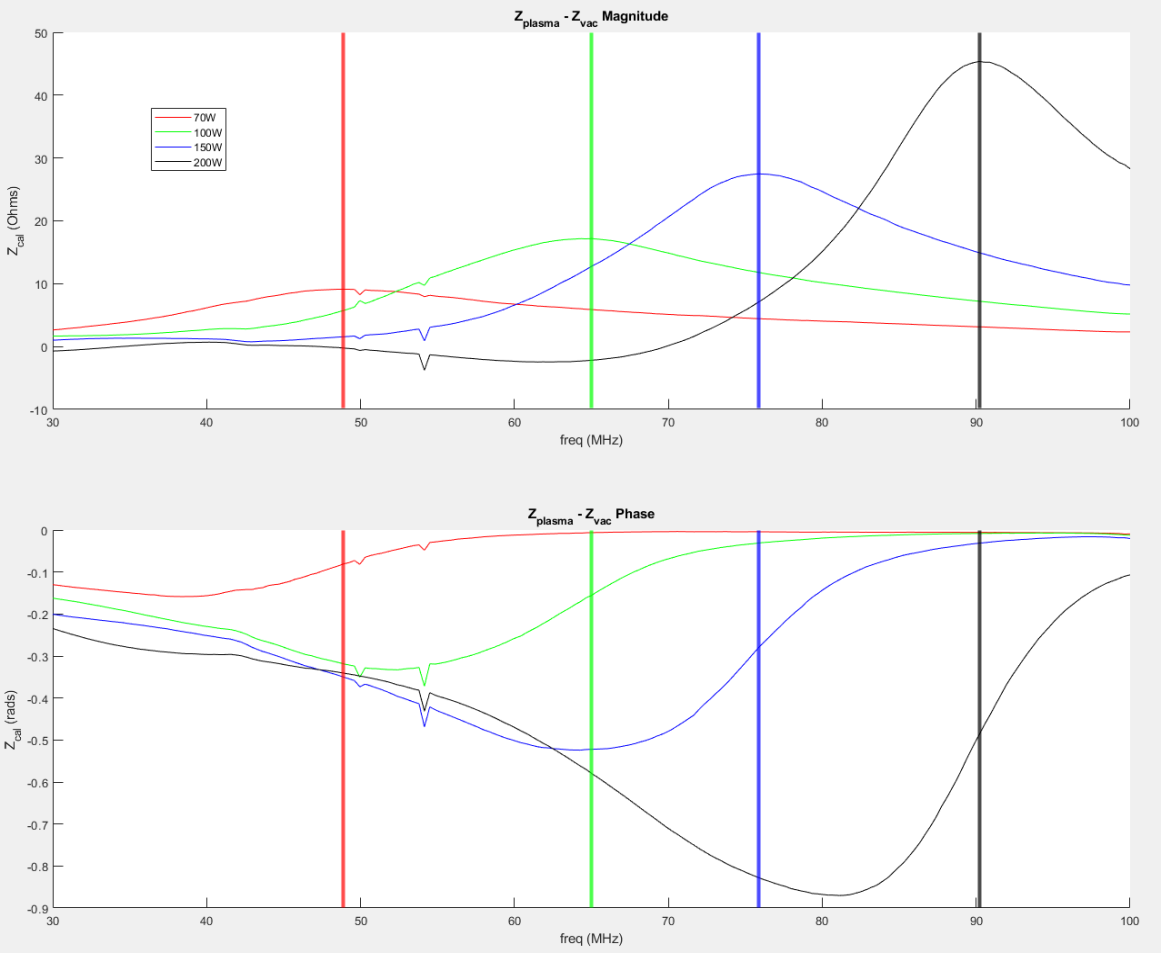

Figure 18. Magnitude and phase of antenna-plasma impedance after calibration with several different RF powers. Chamber pressure was 7.5 mTorr. Increasing the RF power causes the parallel resonant frequency to increase.

Next the pressure was held constant at 7.5 mTorr of Argon gas and the RF plasma source power was varied. Figure 18 clearly shows parallel resonance shift to higher frequencies as the RF power increases. This is likely due to the increased power causing more neutrals inside the chamber to become ionized. This creates a more dense plasma which causes the resonant frequencies also increase.

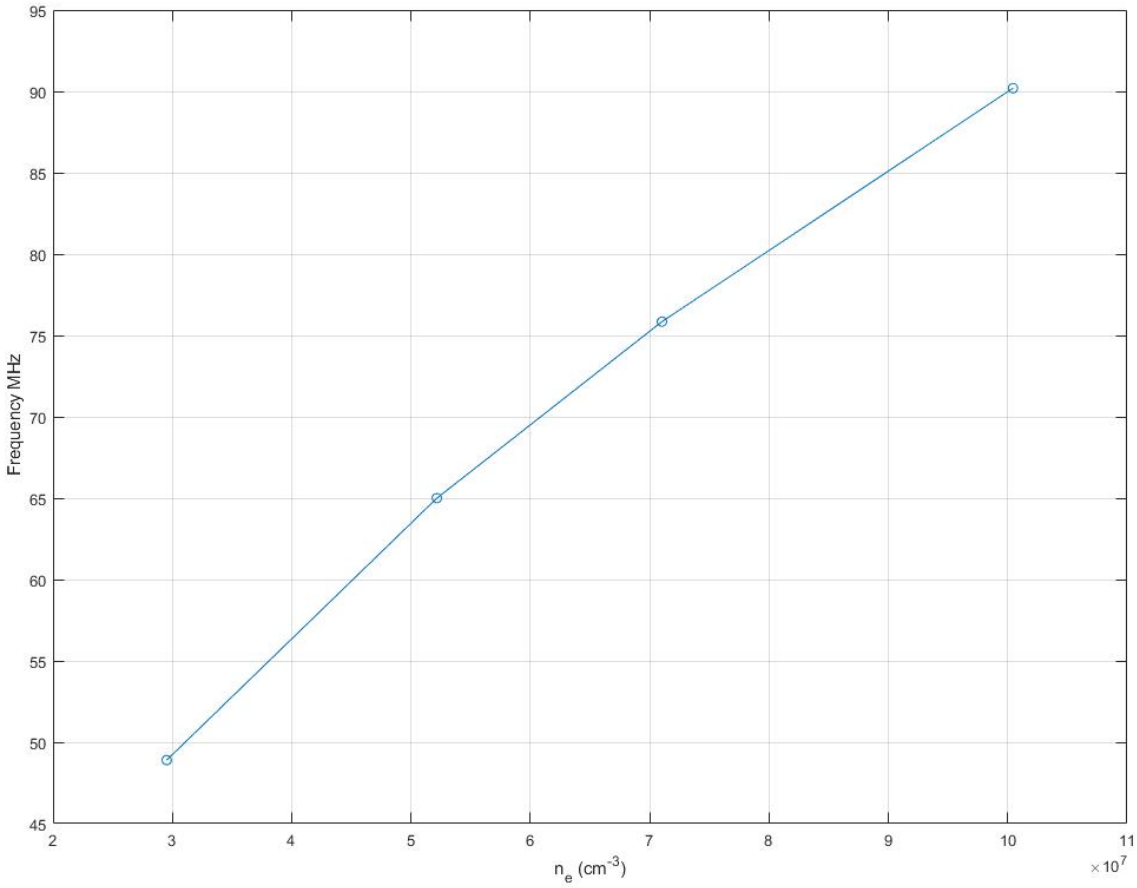

Figure 19. Electron density obtained from plasma frequency impedance measurements. The densities were calculated from the parallel resonant frequencies from Figure 18.

As the parallel resonant frequency increased the electron density increased as well. Equation 2 was used to calculate the electron densities. While these densities are higher than expected in the ionosphere, it is important that this test verified the antenna is capable of impedance measurements.

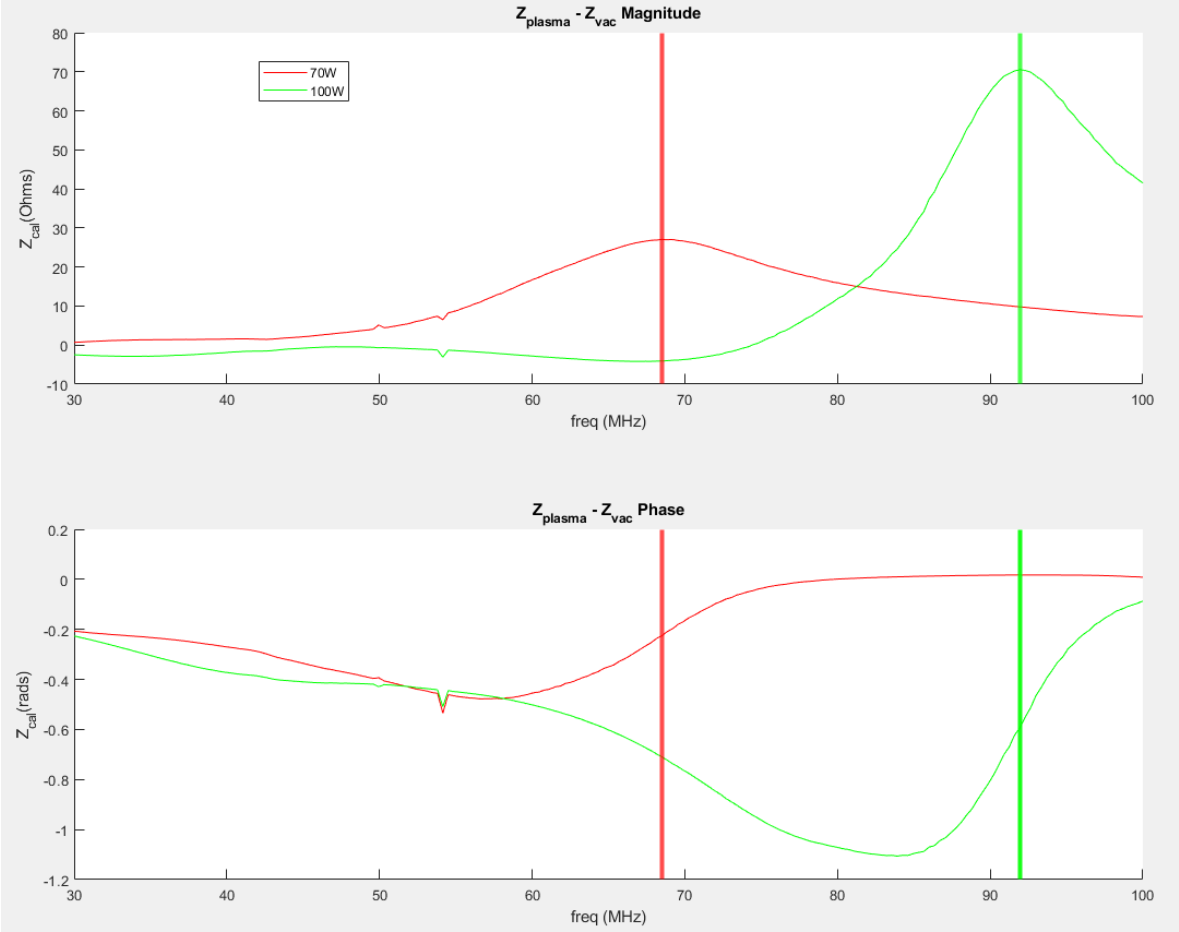

Figure 20. Magnitude and phase of antenna-plasma impedance after calibration with two different RF powers. Chamber pressure was 5 mTorr.

For the next test scenario, the chamber pressure was reduced to 5 mTorr of Argon gas and the process of increasing the RF power to trigger the plasma was repeated. Any RF power higher than 100 Watts was above the selected frequency range and therefore not measured by the network analyzer. As with the previous experiment the parallel resonance increased as the RF power is increased.

Interestingly, the data sets with less pressure in the chamber produced more dense plasmas when the RF power was equal. The 70 W and 100 W results from the 5 mTorr data set compared to the 7.5 mTorr data set clearly show a higher resonant frequency when

the RF power was matched. It is believed that this is due the amount on neutrals present in the chamber and mean free path of the electrons. Less Argon gas in the chamber will decrease the number of ion-neutral collisions and increase the mean free path of the plasma particles. Our impedance probe is placed in the rear most part of the plasma chamber and having a greater mean free path means more plasma reached our probe. When the chamber pressure was set to 10 mTorr, no resonant frequencies were observed due to the excessive number of ion-neutral collisions. Not enough plasma was able to reach the back of the chamber where the probe was located.

4.2 SPADE and iMESA results

SPADE operational impedance data was shared with us by the NRL. The SPADE data was analyzed in order to understand what range of plasma densities expected for the impedance payload in operation. The impedance payload will operate at an altitude comparable to the ISS. SPADE data collected on 15 September 2020 was analyzed. SPADE measured the impedance using the RF-IV method, similar to how our impedance probe operates. The raw data included frequency, RF voltage, quadrature voltage, RF current, and quadrature RF current. Using Equation 22 the data is converted into an uncalibrated impedance spectrum. Then the calibration process was performed and the data analyzed.

iMESA data was collected over a similar timeframe as SPADE on the same day 15 September 2020. iMESA is an electrostatic plasma analyzer while the SPADE is an impedance probe. Plasma density was analyzed with two separate sources using two different techniques. Showing that both iMESA and SPADE produced similar results while

both operating on the ISS provides us with the confidence that the measured densities were accurate.

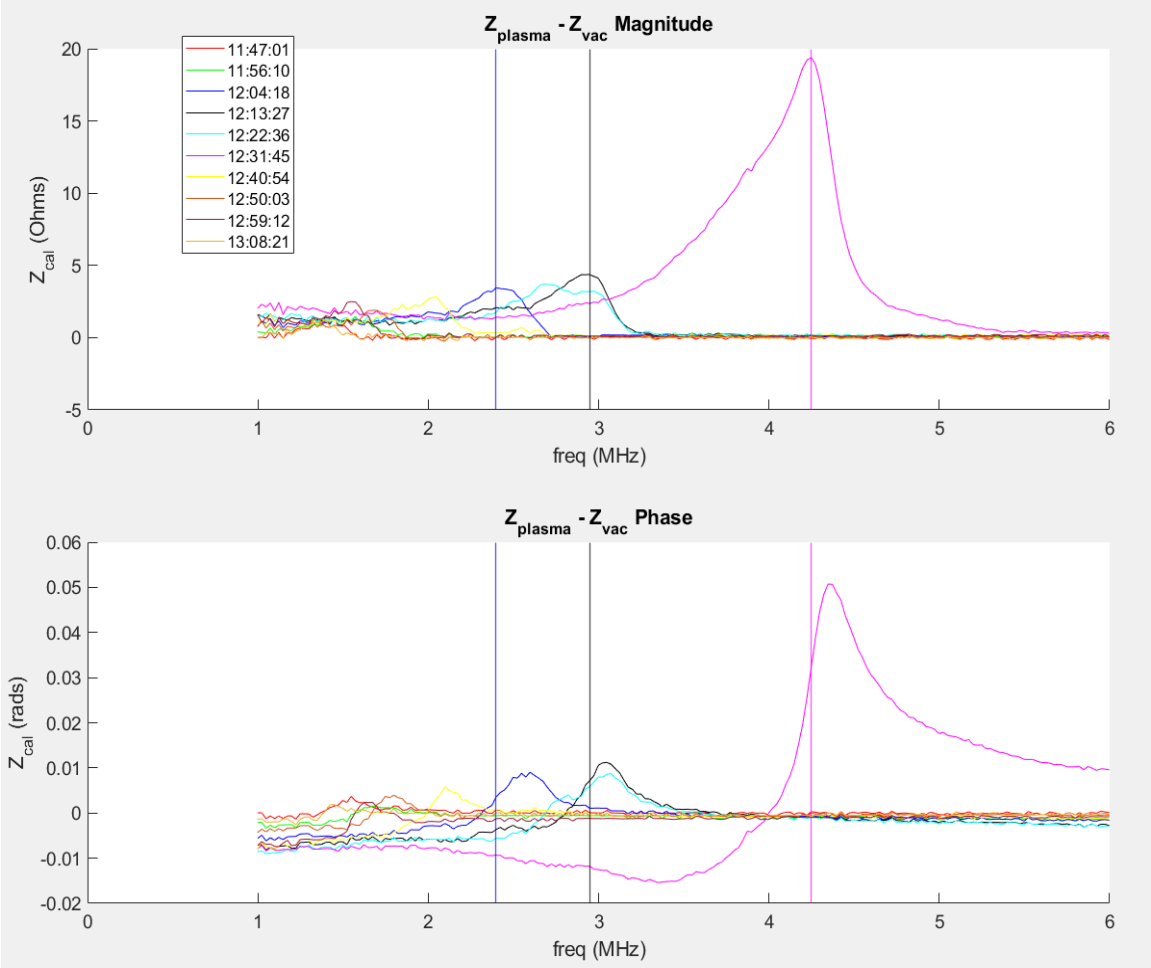

Figure 21. Calibrated magnitude and phase of plasma-SPADE impedance measured from the ISS on 15 September 2020. The legend lists the time in UTC of each measurement and represents a roughly 90-minute timeframe or one ISS orbit. 12:31:45 UTC shows the largest impedance measurement.

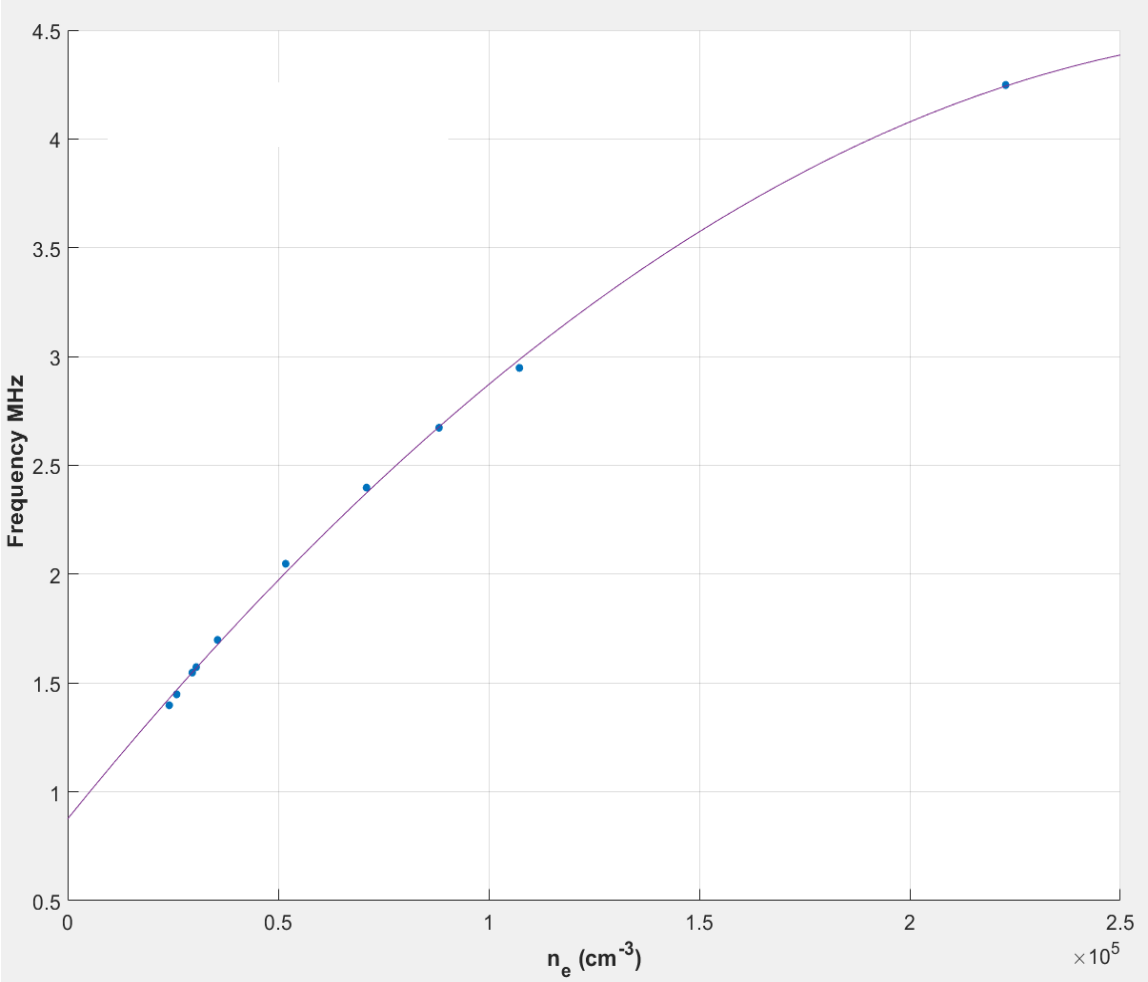

Figure 22. SPADE Electron density measured from plasma frequency impedance measurements. These densities were measured from 11:47:01 UTC to 13:08:21 UTC on 15 September 2020.

The ISS takes about 90 minutes to orbit the Earth. The roughly 90-minute timeframe with approximately 10 minutes per data set represent an average range in densities the ISS experiences. The SPADE data showed plasma electron densities at the ISS ranging from $2.50 \times 10^4\ cm^{-3}$ in the full night side of the Earth to $2.23 \times 10^5\ cm^{-3}$

in the daylight side. Therefore, we should expect to see similar plasma density ranges for our impedance payload during operations.

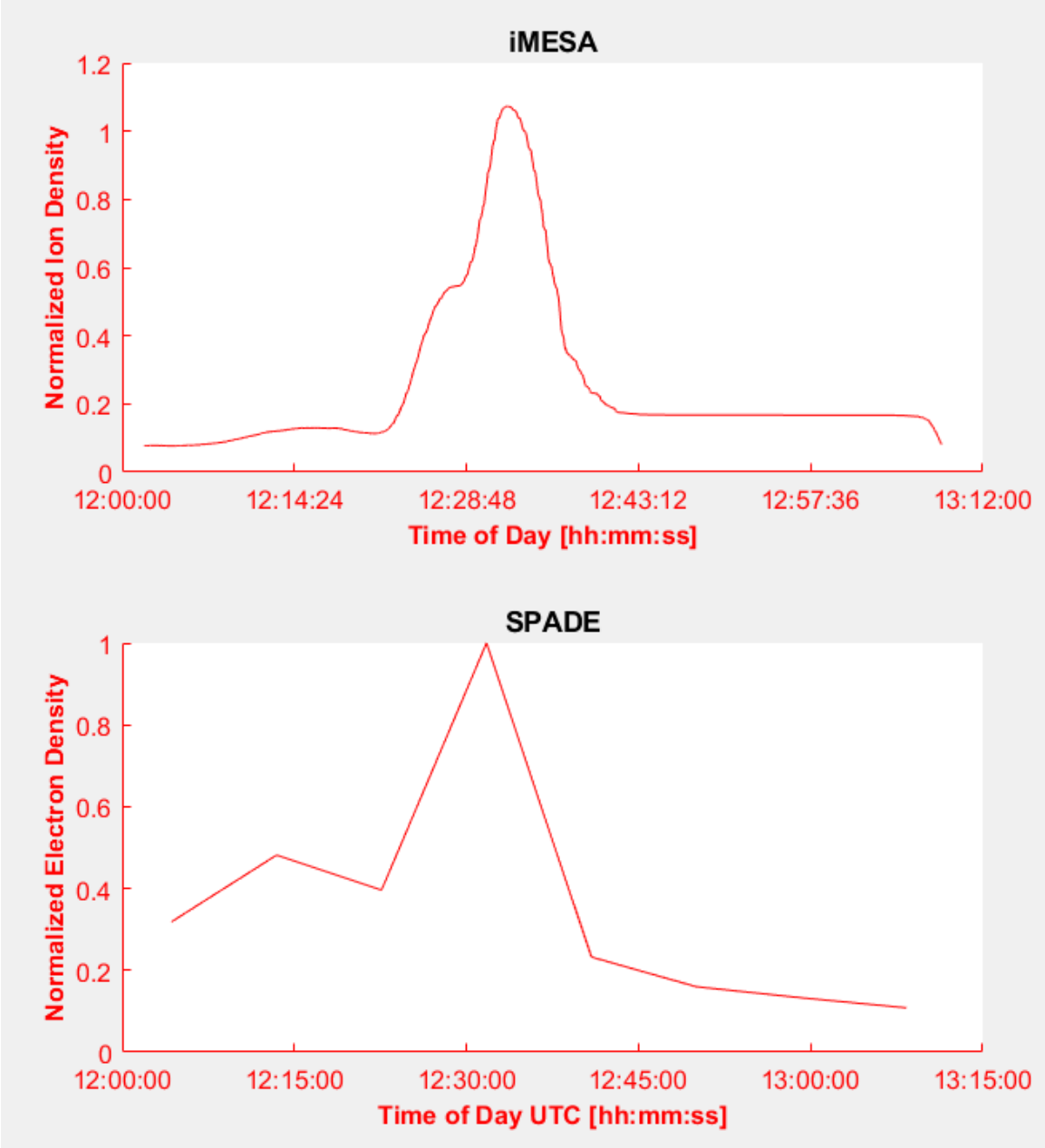

Figure 23. Normalized and smoothed plot of iMESA plasma density measurements and a sample of SPADE data. Both data sets are from onboard the ISS over a similar timeframe in UTC. These plots represent roughly one ISS orbit around Earth to provide a decent range of densities at that altitude of the ISS.

4.3 Impedance circuit board bench test

After verifying the antenna connected to a network analyzer is capable of impedance measurements the IP circuit board was tested using the procedures outlined in Section 3.9. Table 3 contains the input parameters for this experiment.

Table 3. Impedance Probe Bench Test Input Values

Measured resistor	50 Ω
Measured capacitor	1.8 pF
Measured inductor	1 μH
Frequency range	1 MHz – 10 MHz
Number of data points in each frequency sweep	150

The Arduino was programmed to sweep the frequency with the number of points listed in Table 3. Arduino IDE software was used as the serial monitor and the Arduino was plugged in a laptop using a USB-mirco cable to supply power. The Arduino pins were soldered to the connector that attaches to the IP circuit board. The laptop initiated the serial monitor software and the IP started RF I-V measurements. After several iterations with the code and verifying the cable connections we have not been successful in producing RF I-V data. The error is believed to be a coding issue and not a limitation of our hardware and efforts to correct the issue are ongoing.

Despite being currently unable measure impedance using the IP we are confident the probe will work as intended. The antenna test using a network analyzer demonstrates the functionality of the dual-strap antenna over a large frequency range. Our results on Figure 19 demonstrate our antenna is capable of measuring resonant frequencies with a maximum resolution of 16 MHz and minimum resolution of 11 MHz. Looking at just a

small sample of SPADE data Figure 21 shows the IP will need to measure resonant frequencies with a minimum resolution of around 0.13 MHz to a maximum resolution of 2.2 MHz. There is no hardware or circuitry limitation that should prevent the IP from measuring lower frequencies with the range and sensitivity needed to accurately sample typical ionospheric plasma densities 10^5 cm^{-3} which correspond to 1-5 Mhz.

Figure 23 shows two separate methods of measuring the plasma density onboard the ISS. Over a similar timeframe both SPADE and iMESA measured very similar results which gives us confidence in the accuracy of their results. Coupling the accuracy of their plasma density measurements with our ability to measure resonant frequencies to a sensitivity on par with SPADE provides us with the trust that our IP will be successful in future work.

V. Conclusions

The primary efforts for this research can be summarized as follows: design and build an impedance probe with a unique dual strap dipole antenna, test the antenna and impedance probe in a scaled ionospheric plasma chamber, analyze SPADE data to determine the plasma density at the region our future CubeSat will operate in. The experiments offered a proof of concept for a never before used antenna design and showed us that our impedance probe will be capable of measuring plasma densities in the ionosphere.

The results from this research effort confirm that the dual strap antenna proof of concept is a success. The antenna can perform impedance measurements in a plasma environment and demonstrated the ability to accurately measure plasma densities. SPADE and iMESA both measured comparable plasma densities at the same ISS orbit which provides us with expected densities our impedance probe will operate in. We are confident our impedance probe with the dual strap antenna is capable of measuring plasma densities with the sensitivity on par with SPADE.

Future work for this effort will involve the RF-IV measurement of the IP in a plasma chamber with densities comparable to the ionosphere. Once the Arduino code is completed the IP will be tested at the AFRL plasma chamber. Lab personnel at AFRL recently found a method to reduce the chamber density by two orders of magnitude providing near ionospheric levels.

Additional future work for this effort will focus on the USCGA CubeSat mission for 2021. The CubeSat will contain the impedance circuit board and dual strap dipole antenna that was used in this experiment. The CubeSat will have a different bus than the

ThinSat. Testing and engineering the impedance payload with the new bus will be needed for the CubeSat. If the CubeSat successfully measures electron densities in the ionosphere with the impedance payload then additional impedance spacecraft should be considered. We will have demonstrated how a small payload with minimal power and weight requirements can provide accurate real-time in-situ plasma density measurements. This will provide the space weather community with better modeling data to increase our space weather forecasting.

Appendix A

Collisionless energy transfer due to Kinetic Theory

One of the most significant discoveries from studying the kinetic effects on plasma waves is that in a collisionless plasma there is damping effect known as Landau's damping (Goldston, 1995). Landau's damping was mathematically proven by doing a Laplace transformation of the linearized Vlasov equation for electrons in an unmagnetized plasma. In order to linearize Vlasov's equation we are assuming small amplitude waves. Large amplitude waves will lead to nonlinear effects. The linearized Vlasov's equation is

$$\frac{\partial f_1}{\partial t} + v\frac{\partial f_1}{\partial x} - \frac{e}{m}E\frac{\partial f_0}{\partial v} = 0, \tag{29}$$

where f_0 and f_1 are the unperturbed and perturbed Maxwellian distribution function respectively. The Laplace transform of $f_1(v,t)$ is

$$\widetilde{f_1}(v,s) = \int_0^\infty f_1(v,t)e^{-st}dt. \tag{30}$$

Equation 30 converts some perturbed distribution from temporal to an arbitrary complex frequency s. Substitute $i\omega$ for $\frac{\partial}{\partial t}$ and it for $\frac{\partial}{\partial x}$ in Equation 29 then take the Laplace transform of a time derivative to obtain,

$$(s + ikv)\widetilde{f_1}(v,s) - \frac{e}{m}\tilde{E}\frac{\partial f_0}{\partial v} = f_0(v,0). \tag{31}$$

After a Laplace transform of the Poisson equation and some additional algebra, the dispersion function becomes,

$$\mathrm{D(k,s)\widetilde{E}(s)} = \frac{\mathrm{ie}}{\mathrm{k}\,\epsilon_0}\int_{-\infty}^{\infty}\frac{\mathrm{f_1(v,0)}}{\mathrm{s+ikv}}\mathrm{dv} \tag{32}$$

Equation 12 tells us how the electric field evolves in time given some initial perturbation $f_1(v,0)$ (Goldston, 1995). In order to obtain an expression of the electric field as time progresses $E(t)$ then an inverse Laplace transform of $\tilde{E}(s)$ in needed,

$$E(t) = \frac{1}{2\pi i}\int_C \tilde{E}(s)\, e^{st} ds. \tag{33}$$

In order to complete Landau's treatment, we must identify all possible singularities that may arise from Equation 32 when $v = {\omega}/{k}$. Out of the three types of singularities that arise the only one of significant interest is the first zero $D(k,s)$ as we move the contour line from the real to imaginary axis. This first zero singularity explains weakly damped oscillations in the plasma waves which occur often (Goldston, 1995).

Next, we replace the arbitrary complex frequency s with $-i\omega$ and include the integration around the pole. The dispersion function is then,

$$D = 1 + \frac{ie^2}{mk\epsilon_0}\left(Pr\int_{-\infty}^{\infty}\frac{{\partial f_0}/{\partial v}}{\omega - kv}dv - \frac{\pi i}{k}\frac{\partial f_0}{\partial v}\bigg|_{v={\omega}/{k}}\right) \tag{34}$$

where Pr is the principle value of the integral,

$$Pr\int_{-\infty}^{\infty} = \lim_{\epsilon\to 0}\left\{\int_{-\infty}^{{\omega}/{k}-\epsilon} + \int_{{\omega}/{k}+\epsilon}^{\infty}\right\}. \tag{35}$$

The rightmost term in Equation 34 is the integration around the pole which is πi times the residue. In the limit $\omega \gg kv$ the principle integral can be expanded,

$$\int_{-\infty}^{\infty} \frac{\partial f_0/\partial v}{\omega - kv} \approx \frac{-nk}{\omega^2}. \tag{36}$$

Using a Maxwellian distribution for f_0 the expanded dispersion function becomes,

$$D = 1 - \frac{\omega_p^2}{\omega^2} + i\left(\frac{\pi}{2}\right)^{\frac{1}{2}} \frac{\omega_p^4}{k^3 v_t^3} e^{\left(-i\frac{\omega_p^4}{k^3 v_t^3}\right)}, \tag{37}$$

where $v_t = (T/m)^{1/2}$. Setting the dispersion relation to zero we arrive at our final expression for the frequency ω of an electron plasma wave,

$$\omega = \omega_p - \frac{i}{2}\left(\frac{\pi}{2}\right)^{\frac{1}{2}} \frac{\omega_p^4}{k^3 v_t^3} e^{\left(-\frac{\omega_p^2}{2k^2 v_t^2}\right)}. \tag{38}$$

By properly investigating plasma waves with Landau's treatment, it shows that all plasma waves are slightly damped (Goldston, 1995). Damping in collisionless plasma is due to the particle-wave interaction as electrons near the phase velocity find resonance with the wave. Resonant electrons travel at approximately the same speed of the wave which enables them to effectively exchange energy with the plasma wave. If an electron is slightly slower than the phase velocity, then the wave will transfer energy to the particle causing the wave to slow down and become damped. If the electron is slightly faster than the phase velocity, then the opposite occurs where energy is transferred from particle wave causing the wave to grow.

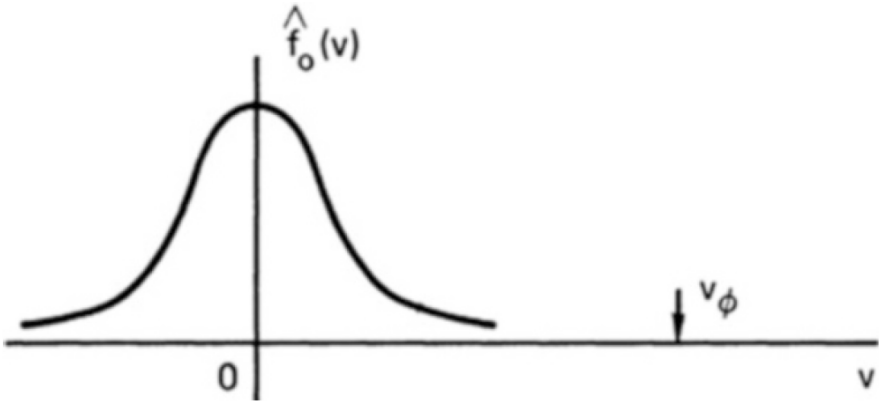

Figure 24. Normalized Maxwellian distribution for the case $v_\phi \gg v_t$

For a Maxwellian distribution there are a greater number of electrons to the left of the phase velocity where $v < v_\phi$. Therefore, there will be a net damping effect as more energy is transferred from the plasma wave (Chen, 2013).

Applying kinetic theory with Landau's treatment captures more details about the plasma than using just MHD. However, kinetic theory significantly increases the difficulty in solving equations and requires much more computational power. While the ThinSat will not require a kinetic treatment of the ionospheric plasma to calculate the impedance, it will be important make sure any future impedance mission properly models the plasma.

Bibliography

Agilent Impedance Measurement Handbook (4th ed.) Agilent Technologies (2013)

Auciello, O., Flamm, D. L. Plasma Diagnostics Volume 1 *Discharge Parameters and Chemistry.* Academic Press.

Balmain, K. "The impedance of a short dipole antenna in a magnetoplasma," in *IEEE* Transactions on Antennas and Propagation, vol. 12, no. 5, pp. 605-617, September 1964.

Bilen, S. G., Haas, J. M., Gulczinski, F. S., Gallimore, A. D. (1999). Resonance-Probe Measurements of Plasma Densities in Electric-Propulsion Plumes. 35th AIAA Joint Propilsion Conference.

Blackwell, D. D., Walker, D. N., Messer, S. J., & Amatucci, W. E. (2005). Characteristics of the plasma impedance probe with constant bias. Physics of Plasmas, 12(9), 093510.

Blackwell, D. D., Walker, D. N., Messer, S. J., & Amatucci, W. E. (2007). Antenna impedance measurements in a magnetized plasma. II. Dipole antenna. Physics of Plasmas, 14(9), 092106.

Blackwell, D. D., Walker, D. N., & Amatucci, W. E. (2005). Measurement of absolute electron density with a plasma impedance probe. Review of Scientific Instruments, 76(2), 023503.

Blackwell, D. D., Walker, D. N., Messer, S. J., & Amatucci, W. E. (2007). Antenna impedance measurements in a magnetized plasma. I. Spherical antenna. Physics of Plasmas, 14(9), 092105.

Blackwell, D. D., Cothran, C. D., Walker, D. N., Tejero, E. M., Gatling, G. R., Enloe, C. L., & Amatucci, W. E. (2015). Advances in Impedance Probe Applications and Design in the NRL Space Physics Simulation Chamber. IEEE Transactions on Plasma Science, 43(8, Part 3), 2649–2657.

Boris, D. R., Fernsler. R. F., Walton, S. G. (2011). The LC resonance probe for determining local plasma density. Plasma Sources Science & Technology, 20(2), 025003.

Chen, F. F. (2003) Langmuir Probe Diagnostics. Mini-Course on Plasma Diagnostics, IEEE-ICOPS meeting.

Chen, F.F, (2015). Introduction to Plasma Physics and Controlled Fusion (3rd ed.). Springer.

Gahan, D., & Hopkins, M. B. (2007). Electrical characterization of a capacitive rf plasma sheath. Review of Scientific Instruments, 78(1), 016102.

Goldston, R. J., & Rutherford, P. H. (1995). Introduction to Plasma Physics (1st ed.). CRC Press.

James, R. W., Freeman, R. W., Allen, L. A., Tejero, E., Kay, B., Kang, J. S. (2020) SmallSat Platform Development for Coast Guard Academy Collaborative Space-Based Research. 34th Annual Small Satellite Conference.

Kelley, M. C., (2009). The Earth's Ionosphere Plasma Physics and Electrodynamics (2nd ed.). Academic Press.

Kline, J. L., Scime, E. E., Keiter, P. A., Balkey, M. M., & Bolvin, R. F. (1999). Ion heating in the HELIX helicon plasma source. Physics of Plasmas, 6(12), 4767.

Ku, V. P. T., & Annaratone, B. M. (1998). Plasma-sheath resonances and energy absorption phenomena in capacitively coupled radio frequency.. Journal of Applied Physics, 84(12), 6546.

Levitskii, S.M., Shashurin, I. P. Sov. Phys. Tech. Phys. 8, 319(1963).

Lieberman, M. A., Lichtenberg, A. J. (2005) Principles of Plasma Discharges and Materials Processing (2nd ed.). Wiley-Interscience.

Maldonado, C. A., Cress, R., Gresham, P., Armstrong, J. L., Wilson, G., Reisenfeld, D., Larsen, B., Balthazor, R. L., Harley, J. and McHarg, M. G. (2020), Calibration and Initial Results of Space Radiation Dosimetry Using the iMESA-R. Space Weather, 18.

Merlino, R. L. (2007). Understanding Langmuir probe current-voltage characteristics. American Journal of Physics, 75(12), 1078–1085.

Nikitin, P., & Swenson, C. (2001). Impedance of a Short Dipole Antenna in a Cold Plasma. IEEE Transactions on Antennas & Propagation, 49(10), 1377.

Patra, S., & Spencer, E. A. (2013). Plasma Impedance Probe: Simulations and Comparison to Sounding Rocket Mission Data. IEEE Transactions on Plasma Science, 41(1), 220–231.

Pisacane, V. L. (2008). The space environment and its effects on space systems. AIAA Press.

Russell, C. T., Luhmann, J. G., & Strangeway, R. J. (2016). Space Physics: An Introduction. Cambridge University Press.

Schunk, R. and Nagy, A. (2009). Ionospheres: physics, plasma physics, and chemistry.

Cambridge University Press.

Spencer, E., Clark, D., & Vadepu, S. K. (2019). A Time-Domain Impedance Probe for Fast Measurements of Electron Plasma Parameters in the Ionosphere. IEEE Transactions on Plasma Science, 47(2), 1322–1329.

The NESC 2016 Technical Update (2016). https://www.nasa.gov/nesc/technicalupdates

Walker, D. N., Fernsler, R. F., Blackwell, D. D., Amatucci, W. E., & Messer, S. J. (2006). On collisionless energy absorption in plasmas: Theory and experiment in spherical geometry. Physics of Plasmas, 13(3), 032108.

Walker, D. N., Blackwell, D. D., & Amatucci, W. E. (2015). Electron density dependence of impedance probe plasma potential measurements. Physics of Plasmas, 22(8), 1–12.

Ward, J., Swenson, C., & Furse, C. (2005). The Impedance of a Short Dipole Antenna in a Magnetized Plasma Via a Finite Difference Time Domain Model. IEEE Transactions on Antennas & Propagation, 53(8), 2711–2718.

Zechar, N. E., "Experimental Investigation of a Parametric Excitation of Whistler Waves" (2017). Wright State University, Dayton OH.